International Soil and Water Conservation Research xxx (xxxx) xxx

Contents lists available at ScienceDirect

International Soil and Water Conservation Research

journal homepage: www.elsevier.com/locate/iswcr

Original Research Article

HOTSED: A new integrated model for assessing potential hotspots of sediment sources and related sediment dynamics at watershed scale

Manuel La Licata [a, b, *], Alberto Bosino [c], Seyed Hamidreza Sadeghi [d, a], Mattia De Amicis [c], Andrea Mandarino [e, f], Andrea Terret [g], Michael Maerker [a, b, h]

[a] Department of Earth and Environmental Sciences, University of Pavia, Via Ferrata 1, 27100, Pavia, Italy
[b] Institute of Geosciences and Earth Resources, National Research Council of Italy, Via Ferrata 1, 27100, Pavia, Italy
[c] Department of Earth and Environmental Sciences, University of Milano-Bicocca, Piazza della Scienza 1, 20126, Milano, Italy
[d] Department of Watershed Management Engineering, Faculty of Natural Resources, Tarbiat Modares University, Noor, Mazandaran Province, Iran
[e] Department of Earth, Environment, and Life Sciences, University of Genova, Corso Europa 26, 16132, Genova, Italy
[f] Geoscape Soc. Coop., Geo-Environmental Consulting, Spin-Off of the University of Genova, Via Varese 2, 16122, Genova, Italy
[g] Consorzio di Bonifica di Piacenza, Strada Valnure 3, 29122, Piacenza, Italy
[h] Working Group on Soil Erosion and Feedbacks, Leibniz Centre for Agricultural Landscape Research (ZALF), Eberswalder Straße 84, 15374, Müncheberg, Germany

ARTICLE INFO

Article history:
Received 26 February 2024
Received in revised form
12 June 2024
Accepted 15 June 2024

Keywords:
Sediment sources identification
Sediment connectivity
Sediment dynamics assessment
Integrated model
Sediment-related hazard map

ABSTRACT

In this paper we introduce HOTSED, a novel, innovative GIS-based model designed for assessing potential hotspots of sediment dynamics at watershed scale. HOTSED integrates geomorphic spatial information with both structural and functional properties of connectivity. HOTSED provides a single and intuitive output that depicts the location of sediment source hotspots. Moreover, it enables the identification of "relative hazard" classes for sediment production and related effects. The general methodological framework is based on the initial elaboration of an Inventory Map (IM) of sediment-related landforms and processes, along with the implementation of a corresponding database. Subsequently, we used data stored in the IM to estimate the geomorphic Potential of Sediment Sources (PSS) through a relative scoring system. Furthermore, we computed Structural Sediment Connectivity (STC) and the Potential for Sediment Transport (PST) by combining terrain and hydrological parameters, vegetation roughness, and rainfall erosivity. Afterwards, PSS, STC, and PST components are integrated through a raster-based calculation method yielding the HOTSED model. We tested the HOTSED procedure in the upper Val d'Arda-Mignano watershed, which is a representative geomorphologically highly active Mediterranean area of the Northern Apennines (Italy). Through photointerpretation, terrain analysis, and fieldwork, we mapped sediment-related geomorphic features for a total of 4640 ha including: badlands and gullies (0.26%), rill-interrill erosion (15.03%), fluvial erosion (0.03%), landslides (70.06%), litho-structural erosional systems (0.87%), slope deposits (12.56%), and alluvial deposits (1.19%). HOTSED revealed hotspots with a very high hazard potential located near main channels or upstream of the reservoir. These areas are often linked with active landslides highly connected to the drainage system and frequently associated with other processes like bank erosion or surficial soil erosion. The model also highlighted linear hotspots corresponding to drainages flowing alongside or intersecting complex geomorphic systems such as landslides. Furthermore, HOTSED identified areas where sediments are stored in depositional landforms, exhibiting a low hazard potential, considering both low geomorphic potential and sediment connectivity. Our conceptual model is generally applicable but proves to be particularly effective in areas characterized by complex and polygenetic geomorphic systems, such as the Northern Apennines. HOTSED offers a valuable tool for watershed authorities to support sustainable watershed and reservoir management.

* Corresponding author. Department of Earth and Environmental Sciences, University of Pavia, Via Ferrata 1, 27100, Pavia, Italy.
E-mail address: manuel.lalicata01@universitadipavia.it (M. La Licata).

https://doi.org/10.1016/j.iswcr.2024.06.002

Abbreviations

AD	Alluvial deposits (sub-database)
ap	Present activity of the primary landform (attribute)
BE	Fluvial erosion (sub-database)
BG	Badlands and Gullies (sub-database)
CN	Channel Network
dp	Sediment sources and dynamics (attribute)
cp	Subordinate processes (attribute)
es	Past trend of evolution of the geomorphic system (attribute)
FS	Final relative Score
GE	Geomorphic Entity
GSSS	Geological, Seismic and Soil Survey
HOTSED	Hotspots of sediment sources and related dynamics (model acronym)
HPD	Hazard Map of Sediment Production and Delivery
HSS	Hotspot areas of Sediment Sources and delivery
IC	Index of Connectivity
IFFI	Italian Landslide Inventory
IM	Inventory Map
ISPRA	Italian Institute for Environmental Protection and Research
LD	Landslides (sub-database)
LR	Litho-structural-erosional systems (sub-database)
PS	Provisional relative Score
PSS	Potential of Sediment Sources
PST	Potential for Sediment Transport
QD	Quaternary deposits
RER	Emilia-Romagna Region
RI	Rill-Interrill erosion (sub-database)
(R)USLE	(Revised) Universal Soil Loss Equation
SD	Slope deposits (sub-database)
SDR	Sediment Delivery Ratio
sp	Secondary processes (attribute)
STC	Structural Sediment Connectivity
STD	Standard Deviation
VSMT	Versus Square Matrix Table
WMS	Web Map Services.

1. Introduction

Mediterranean agroecosystems are notably susceptible to land degradation due to the interplay of climatic factors, anthropogenic pressure, unsuitable agricultural land management, and socio-economic changes (García-Orens et al., 2012, 2013; Lizaga et al., 2019). Actually, land use and climatic changes are affecting the provision of vital ecosystem services in both agricultural and forest lands (Cerdà et al., 2018; Martín-López et al., 2016; Nieto-Romero et al., 2014). They also influence natural geomorphic processes such as landsliding and various forms of soil erosion (Cendrero et al., 2020; Costantini & Lorenzetti, 2013; Lizaga et al., 2018; Olsson et al., 2019; Pepe et al., 2019). These processes generate both on-site and off-site impacts (Borrelli et al., 2018; FAO, 2019; Ferreira et al., 2022), such as soil properties degradation, nutrient depletion, and diminished soil water retention capacity (Li & Fang, 2016). Moreover, soil erosion plays a major role for sediment dynamics at watershed scale (*e.g.*, López-Vicente & Navas, 2010; Borrelli et al., 2014; Bosino et al., 2022), thus, highlighting the key role of watershed management in both restoring sediment-starved rivers and mitigating sediment-related critical issues, such as reservoir siltation and water quality degradation (Chen et al., 2020; Kondolf & Podolak, 2014; Verstraeten et al., 2006).

Therefore, identifying the location, extent, and distribution of hotspot areas of sediment dynamics and assessing their main natural and/or anthropogenic drivers is a prerequisite to implement sediment control measures in watersheds affected by land degradation (Le Houérou, 1993; Lizaga et al., 2020; Schmaltz et al., 2024). Generally, a preliminary key step involves assessing the distribution of sediment sources relative to the channel network (Gellis et al., 2016). Once sediment source areas are identified, it is essential to establish sediment transfer patterns from sources to sinks (Cho et al., 2023; Dumitriu et al., 2017; Fryirs, 2013).

Sediment connectivity plays a pivotal role in evaluating sediment dynamics for watershed and river management (Brierley et al., 2006; Hooke et al., 2021; Najafi et al., 2021a; Wainwright et al., 2011). In this paper, we refer to connectivity as a crucial property of the system that reflects the strength and continuity of sediment links between system components at a given point in time (Heckmann et al., 2018; Wohl et al., 2019). The degree of linkage thereby controls the source-to-sink transfer of sediments based on how sediments move among the geomorphic units, *i.e.*, on hillslopes, between hillslopes and channels, and within channels (Bracken et al., 2015).

Connectivity exhibits two inherent properties, known as structural and functional connectivity. The former emerges from the spatial arrangement of system components and their physical linkages in the landscape. The latter refers to the actual transfer of water and sediments across the landscape, based on dynamic processes active within the system (Heckmann et al., 2018). However, while most studies have focused on assessing the intensity and degree of structural connectivity (Najafi et al., 2021a; Yu et al., 2023), a limited number of studies have quantified also functional components (*e.g.*, Liu & Fu, 2016; Grauso et al., 2018; Zingaro et al., 2019; Najafi et al., 2021b). Anyway, coupling soil erosion and sediment connectivity modelling has turned out to be a promising approach to represent both structural and functional variability of sediment-related processes (*e.g.*, Mahoney et al., 2021; Hao et al., 2022). In this context, the combination of the Sediment Delivery Ratio (SDR) concept (Walling, 1983) has proven to be an informative method for evaluating sediment sources and spatio-temporal changes in sediment yield (*i.e.*, the 'RUSLE—IC—SDR' approach; Hamel et al., 2017; Zhao et al., 2020; Woznicki et al., 2020; Michalek et al., 2021; Abebe et al., 2023; Guo et al., 2023).

Traditionally, sediment connectivity studies primarily rely on comparing independent results from GIS modelling, field-based assessments, and geomorphological mapping (Hooke & Souza, 2021). Their interpretation and validation usually involve qualitative (*e.g.*, Theler et al., 2010; Cavalli et al., 2013; Zanandrea et al., 2019) and statistical methods (*e.g.*, Messenzehl et al., 2014; Zingaro et al., 2019; Martini et al., 2022). However, we would like to point out a general lack of information on geomorphic processes, their dynamics, and process-form relationships in research related to geomorphological connectivity (Poeppl et al., 2023). Nevertheless, other techniques have recently been applied to extract more information from geomorphic spatial data and connectivity assessments using, *e.g.*, landform response and sediment export quantification (Rainato et al., 2018), or DEM of Difference as well as channel profile analysis (Torresani et al., 2023). Anyway, it remains a common practice to treat geomorphic processes and connectivity as separate system characteristics, often without joining them into an integrated modelling approach. This makes it also difficult to

detect emergent properties of the system—that is, properties that become apparent and result from various interacting components within a system. This is especially true in geomorphologically complex areas where geomorphic processes evolve under environmental and human-induced changes.

An attempt in this direction was made by Heckmann & Schwanghart (2013), which applied a spatially explicit graph model to analyse sediment cascades resulting from the interaction of potential sediment pathways and the corresponding geomorphic process domains (Wichmann et al., 2009). However, despite the fact that their approach provides an integrated way to depict the connectivity of potential areas of occurrence of sediment-related processes, the spatial pattern of process activity delineated by simulation models cannot reproduce in detail the field situation (Heckmann & Schwanghart, 2013). Buter et al. (2022) improved their modelling approach going a step further in defining conditions under which sediment transport processes may occur. However, also in this case the model focuses specifically on functional connectivity, overlooking its structural aspects. Furthermore, Steger et al. (2022) developed a new data-driven approach to identify and map areas that are simultaneously susceptible to debris flow initiation and structurally connected to the channel network in Alpine environments. However, the latter approach is not suitable for addressing geomorphologically complex areas where several diversified processes contribute significantly to sediment dynamics. Recently, Fabre et al. (2024) combined a hillslope erosion model (*i.e.*, WaTEM/SEDEM; Borrelli et al., 2018) with a river network sediment connectivity model (*i.e.*, CASCADE; Tangi et al., 2019) to assess the transport of fine sediments in the fluvial network once they have been produced by surface runoff. However, despite the fact that their approach allows to assess net erosion source areas in large watersheds, along with their contribution to sediment dynamics into a river connectivity framework (*i.e.*, longitudinal connectivity), it lacks actual geomorphological spatial data, leading to a potential underestimation of sediment sources (Fabre et al., 2024). Thus, the latter approach does not represent the geomorphological complexity of a small-medium watershed nor the contribution of geomorphic processes to sediment dynamics based on hillslope-channel connectivity.

Based on the above-mentioned considerations, our paper introduces a novel methodology that addresses the need for an integrated approach encompassing geospatial information on sediment-related geomorphic features, the potential of these features as sediment sources, as well as structural and functional components of watershed-scale connectivity. Hence, our study aims to provide: (i) a new GIS-based multiscale geomorphological mapping procedure for assessing spatial characteristics of sediment-related landforms and processes, as well as (ii) a new integrated GIS-based modelling framework for assessing hotspots of sediment sources and related dynamics at watershed scale. The proposed methodology has been specifically developed for geomorphologically highly active areas characterized by processes that overlay in space and time.

Therefore, we selected the upper Val d'Arda-Mignano watershed, which is a geomorphologically highly active agricultural and forested valley in the Northern Apennines (Italy), to test our approach. The study area is of particular interest concerning land degradation processes, as well as regarding sedimentation in the fluvial system and the reservoir (de Vente et al., 2006; Patro et al., 2022). According to La Licata et al. (2023), the study area represents a landscape laboratory to investigate various processes that produce complex and polygenetic geomorphic systems, influenced by anthropic activities. Furthermore, this paper intends to present the first comprehensive Inventory Map of sediment-related landforms and processes of the upper Val d'Arda.

2. Study area

The upper Val d'Arda is located in the western Emilia-Romagna region, Northern Apennines, Italy (Fig. 1a and b). It coincides with the watershed upstream of the Mignano reservoir (Fig. 1c). The area stretches SW-NE for ~14 km and extends for ~88 km^2, with an altitudinal range varying from 285 to 1356 m a.s.l. (Mt. Menegosa; Fig. 1c). It is drained by the Lubiana creek and Arda river (Fig. 1c).

In the study area, the geological formations belong to the External Ligurian Domain (Conti et al., 2020; Marroni et al., 2001). According to Servizio Geologico d'Italia (1999) and Martini & Zanzucchi, 2000, the main lithological units in the study area consist in: (i) calcareous and silicoclastic marly turbidites, interstratified with arenitic and pelitic layers (*Mt. Cassio Flysch*; Upper Cretaceous); (ii) tectonized varicoloured clays with intercalated layers of turbiditic sandstones (*Cassio Varicoloured Shales*; Upper Cretaceous); (iii) arenaceous-pelitic turbidites made up of lithoarenites and silty marly pelites (*Scabiazza Sandstones*; Upper Cretaceous); (iv) arenaceous-pelitic turbidites alternating with calcareous and marly rocks (*Val Luretta Formation*; Paleocene-Eocene); (v) turbidites made up of calcarenitic marly limestones and marls alternating with arenites and pelites (*Bettola Flysch*; Upper Cretaceous-Paleocene); (vi) argillites with intercalations of turbiditic arenites, calcareous-marly turbidites, or sedimentary and ophiolitic breccias (*Guselli Argillites*; Upper Cretaceous); (vii) arenaceous-pelitic and calcareous-marly turbidites (*Farini d'Olmo Flysch*; Paleocene-Eocene); and (viii) randomly embedded *mélanges* made up of sedimentary and ophiolitic lithofacies and olistoliths of the Pietra Parcellara Complex (Upper Cretaceous).

Due to the sedimentary nature of the main geological formations, landscape evolution is largely controlled by the interaction between the lithological characteristics and local structural features (Pellegrini & Vercesi, 2017). The area is mostly characterized by open slopes composed of pelitic and chaotic units with moderate slope gradients. In contrast, selective erosion acting on more resistant rocks (*i.e.*, interstratified flysch and ophiolitic units) has produced isolated outcrops and very steep rock walls with high relief energy.

Due to the extensive presence of weak clayey rocks (Borgatti et al., 2006), the study area is particularly susceptible to water erosion and landslide processes, which typically interact and overlap. These processes produce complex and polygenetic geomorphic systems that are coevolving with anthropic activities. Landslides are widespread and release sediments into the channel network with a high variability of magnitudes and frequencies. Several of them are complex landslides, which mostly have slide-flow type characteristics (*i.e.*, 'earthflows'; Hungr et al., 2014; Carlini et al., 2016). Large earthflows are considered the most important geomorphic factor in shaping the landscape after the Last Glacial Maximum (Bertolini et al., 2004; Bertolini & Tellini, 2001; Simoni et al., 2013). Both distribution and extent of these landslide bodies have deeply influenced the channel network configuration, as well as the morphological evolution of the fluvial system (La Licata et al., 2023).

Other processes contribute significantly to land degradation. Several active fluvial erosion scarps and retreating banks can be identified along the main channels. Upland rill-interrill erosion is another main source of sediments, particularly on arable lands (Staffilani et al., 2019). Moreover, badlands have a high potential for soil loss and sediment production, even if they are limited in their spatial extent due to peculiar lithological features. They represent one of the most complex soil erosion landforms and are characterized by a set of associated processes like piping, gully erosion, and mudflows that contribute to their development. All above mentioned erosion processes contribute to the sediment delivery to

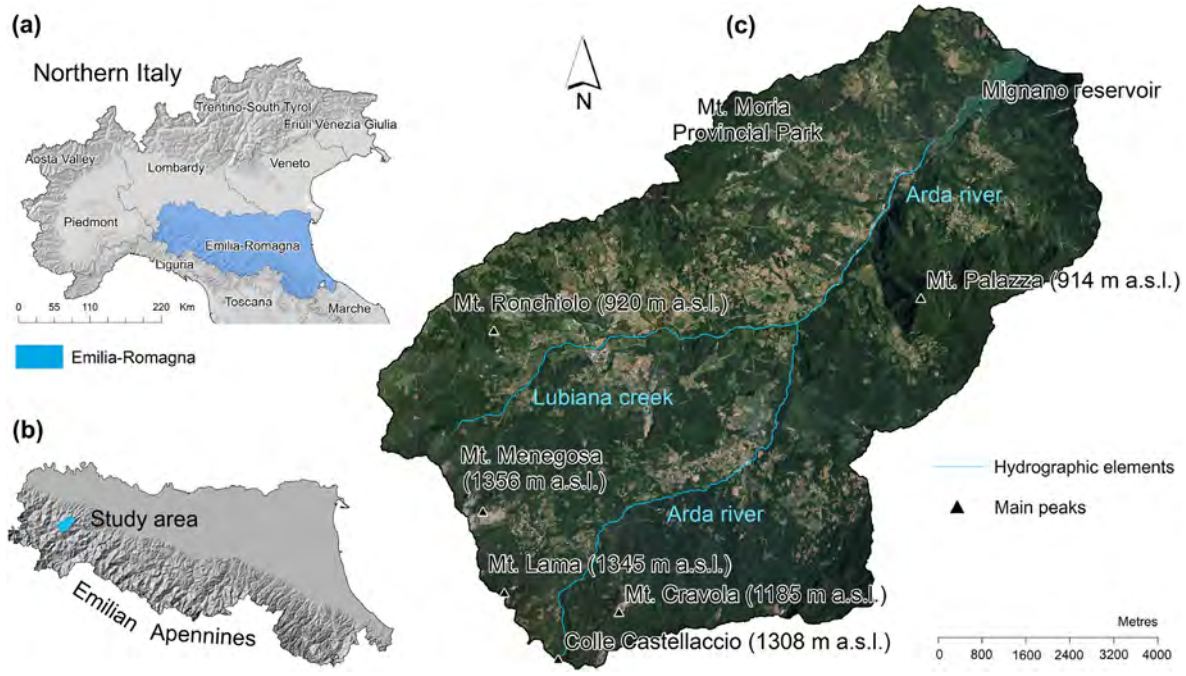

Fig. 1. (a, b) Geographic outline of the study area in the Northern Apennines (Emilia-Romagna region), Italy. (c) The upper Val d'Arda-Mignano watershed. The main elevation peaks and hydrographic elements are represented on the map.

the catchment outlet, depositing large amounts of sediment in the Mignano reservoir (Van Rompaey et al., 2005; de Vente et al., 2006; Patro et al., 2022; Fig. 1c). Nevertheless, the sediment delivery is attenuating over various spatio-temporal scales by different sediment sinks, *i.e.*, depositional systems acting as sediment storages within the watershed such as slope and fluvial deposits.

The climate is humid temperate, with a very low or without water deficit in summer (Cfa and Cfb, Köppen-Geiger climate types; Kottek et al., 2006). The mean annual air temperature is 11.4 °C at lower elevations and 9.7 °C at higher ones. Annual precipitation shows a sub-coastal rainfall regime with a main peak in autumn and a secondary peak in spring. The mean annual rainfall at lower and higher altitudes are respectively 930 mm and 1155 mm. July is the driest month and November is the wettest (La Licata et al., 2023).

Arable lands are widespread, while a few orchards and vineyards are also present (Regione Emilia-Romagna, 1994). Forest vegetation is mostly composed of oak, hornbeam and chestnut woods at lower altitudes, as well as beech woods at higher ones (Camerano, Varese, & Grieco, 2006; Ubaldi et al., 1996). Deciduous, coniferous and mixed coppice woods and high forests are quite extensive.

Soils develop under biochemical alteration and incipient or complete decarbonation. Water erosion processes often affect soils and consequently limit their development. In particular, partially decarbonated soils (*Calcaric Cambisols*) are dominant on marly-calcareous, arenaceous-pelitic, and colluvial parent material, both in forest and agricultural fields, as well as in areas subjected to mass movements and episodic runoff processes. Less developed soils (*Calcaric Regosols*) are present on convex, steep, and erosive slopes with scarce vegetation cover. Soils with stronger profile differentiation, complete decarbonation and mild acidification (*Eutric Cambisols* and *Dystric Cambisols*) are present on more stable slopes, both on calcaric and ophiolitic parent material (Regione Emilia-Romagna, 1994; IUSS Working Group WRB, 2015).

3. Materials and methods

3.1. General methodological framework and main definitions

The general methodological framework consists in the following steps (*i.e.*, 1–6; Fig. 2), which will be further explained in the dedicated sections.

1. A multiscale geomorphological mapping framework is applied to elaborate a comprehensive Inventory Map (IM) within a GIS environment, accounting for the entire range of sediment-related landforms and processes acting as sediment sources within the watershed, following Gellis et al. (2016) and Dumitriu et al. (2017). The mapping framework relies on the identification of 'geomorphic systems' (*i.e.*, hierarchical overlay of processes and landforms), which are manually digitized using polygon features as elementary mapping units. These polygon features are herein defined as Geomorphic Entities (GEs), that are (i) uniquely spatially identifiable geomorphic systems, (ii) consisting of one or multiple overlaying processes producing related landforms, (iii) potentially interacting with watershed hydrology and external drivers, (iv) displaying a certain sediment export independently from their process composition.
   The mapping procedure is specifically adjusted based on data availability, watershed characteristics, and research objectives, as well as the accuracy and resolution of the mapping scale.
2. A hierarchically organized database is implemented to collect information useful to characterize each Geomorphic Entity (GE) for further elaboration. Thus, a series of attributes derived from different spatio-temporal surveying scales is selected to assess the characteristics of GEs which influence sediment dynamics (*e.g.*, process types, process composition, dynamics, activity, evolution). Moreover, spatial and numerical analyses can be performed to evaluate the extent and frequency of the different types of sediment sources within the selected study area.

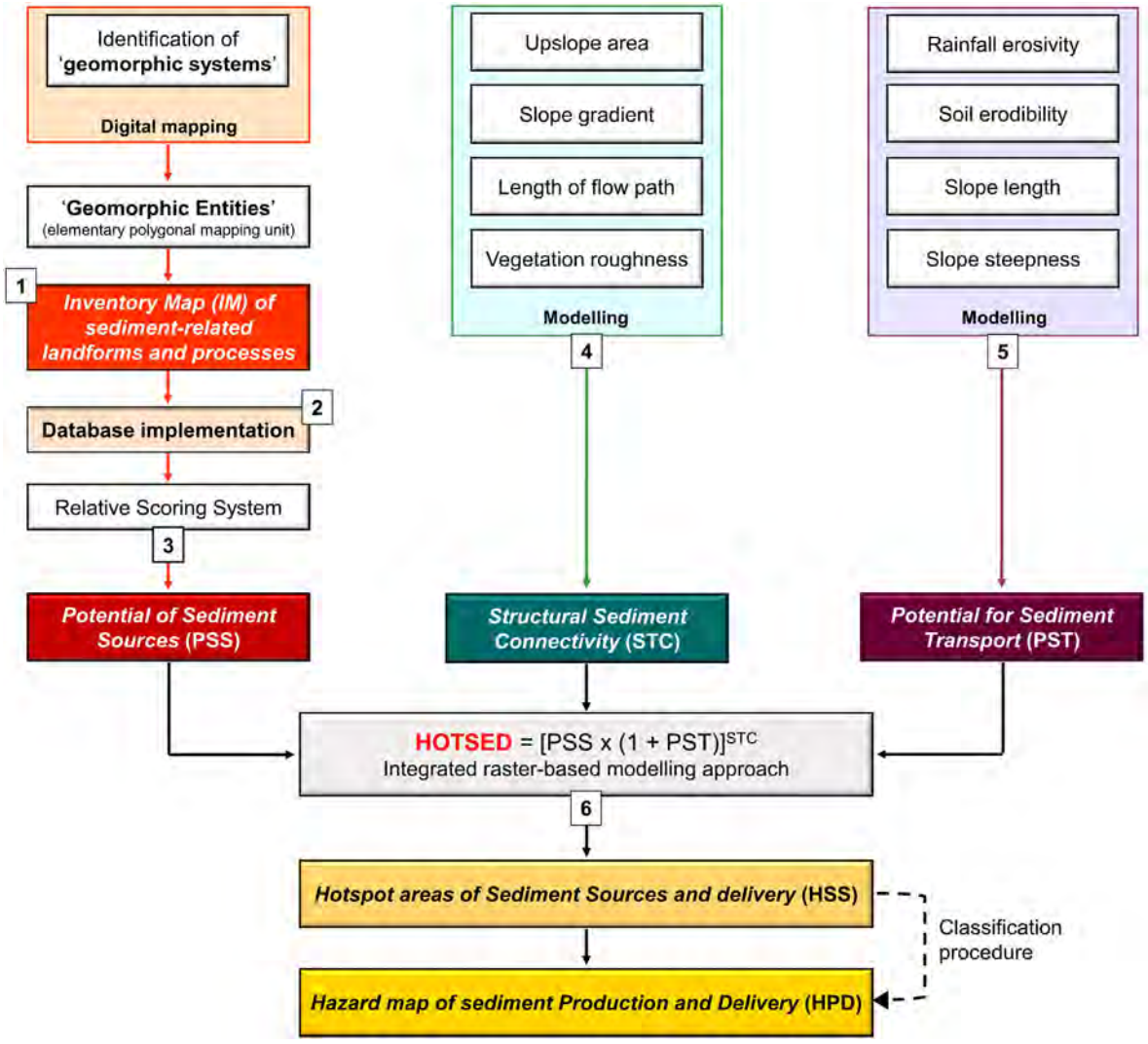

Fig. 2. Flowchart of the general methodological framework that leads to the HOTSED model.

3. The potential of each GE acting as a sediment source is estimated based on information stored in the IM database, adopting a relative scoring system. The relative scoring system takes into account the structure of the database, attribute types, geomorphological setting, and the morphoclimatic conditions of the selected study area. The aggregation, rasterization, and summation of the whole GEs, resulting in a single output map, provide the *Potential of Sediment Sources* (PSS).
4. A watershed-scale morphometric index of sediment connectivity is used to assess the potential degree of connection between hillslopes and selected targets for transported sediments (*e.g.*, Borselli et al., 2008; Cavalli et al., 2013). Land use data are incorporated to derive a dimensionless proxy for impedance to water flow (*i.e.*, vegetation roughness). Different geographic elements (*e.g.*, catchment outlet, drainage network, main channels, lakes, reservoirs, roads, urban areas) can be selected as target features of the model, according to the objectives of the study (Cavalli et al., 2014). The resulting output map provides the *Structural Sediment Connectivity* (STC).
5. The inherent physical potential for sediment delivery from hillslopes is assessed using various environmental input factors commonly employed in other modelling approaches (*i.e.*, USLE-type models; Alewell et al., 2019) as external forcings and intrinsic properties of the landscape. They include rainfall erosivity, soil erodibility, slope length, and slope steepness. The resulting output map provides the *Potential for Sediment Transport* (PST).
6. The different components, namely PSS, STC, and PST, are integrated into a raster-based model (HOTSED). It provides a single output which depicts the location and distribution of the *Hotspot areas of Sediment Sources and delivery* (HSS). Subsequently, a classification procedure is applied to the HSS map in order to obtain a *Hazard map of sediment Production and Delivery* (HPD). More details on the modelling procedure are provided in Section 3.2.8.

3.2. Application of the methodological framework to the study area

3.2.1. Assessment of pre-existing input data

The following databases developed by regional and national authorities were acquired and integrated in a GIS dataframe using the ArcMap v.10.3.1 software (ArcGIS - ©Esri):

- Quaternary deposits, 1:10,000 scale (QD) (SGSS, 2005).
- Italian Landslide Inventory, 1:10,000 scale (IFFI) (APAT, 2007; Trigila et al., 2010).

The QD database was developed by the Geological, Seismic and Soil Survey (GSSS) of the Emilia-Romagna Region (RER) (https://www.geoportale.regione.emilia-romagna.it/). It includes depositional landforms such as slope and alluvial deposits. Moreover, it comprises information on landslide deposits integrating the IFFI inventory (APAT, 2007; Trigila et al., 2010).

The IFFI inventory was developed by the Italian Institute for Environmental Protection and Research (ISPRA; https://www.progettoiffi.isprambiente.it/cartografia-on-line/). It was elaborated integrating historical landslide data, photointerpretation of aerial images, and field surveys (Trigila et al., 2010). For the RER, the survey scale was 1:10,000 (Gozza & Pizziolo, 2007) and the related minimum area for cartographic mapping was 1600 m^2 (Trigila et al., 2007). This implies that spatially limited landslide deposits below the threshold may not have been mapped. Landslide classification is based on Varnes (1978), Cruden and Varnes (1996), IAEG (1990), WP/WLI (1990, 1991, 1993a, 1993b, 1994), and IUGS/WGL (1995). Falls and topples are grouped into the same class (*i.e.*, fall/topple), as well as rotational and translational slides (*i.e.*, roto-translational slide). Most of the landslides within the study area are classified as complex undifferentiated landslides (*i.e.*, landslides characterized by a combination of movements, as well as rock avalanches; SGSS, 2005; Trigila et al., 2007). Landslides in the study area are classified as *Active* or *Dormant* (Cruden & Varnes, 1996; APAT, 2007).

A series of high-resolution orthophotos covering a 44-years period were provided by national and regional Web Map Services (WMS). We obtained the years 1988, 1996, and 2000 from the National geoportal (http://www.pcn.minambiente.it/mattm/servizio-wms/). Years 1976–78, 2008, 2011, 2018, 2020 (Red, Green, Blue; RGB), and 2020 (Near Infrared; NIR) were supplied by RER geoportal (https://www.geoportale.regione.emilia-romagna.it/catalogo/dati-cartografici/cartografia-di-base/immagini).

3.2.2. Terrain analysis

The selected watershed was outlined based on a 5m Digital Terrain Model (DTM) (Regione Emilia-Romagna, 2019) using the SAGA GIS v.8.1.1 software (Conrad et al., 2015). Therefore, several DTM tiles were mosaicked using a B-Spline interpolation algorithm. Subsequently, a quality check using a combination of visual methods and non-spatial statistical visualizations was performed (Maerker et al., 2018; Podobnikar, 2009). The resulting DTM was filtered for errors with a Gaussian Filter of radius 3. Subsequently, it was pre-processed for hydrological modelling by deepening drainage routes using the Sink Removal tool with a threshold height of 10 m. This method was preferred to 'fill sinks' algorithms to avoid the creation of artificial flat areas (Lidberg et al., 2017), especially along the river systems. Afterwards, Flow Directions (Wang & Liu, 2006) and Flow Accumulation (Tarboton, 1997) were computed to derive channel network and watershed. A Strahler order of 5 was used as threshold for the computation of the main channel network (Strahler, 1957).

We carried out a DTM-based terrain analysis to characterize the main land-surface features useful for landform identification (Olaya & Conrad, 2009). Therefore, we computed the analytical hillshading and some primary morphometric parameters such as slope, aspect, profile curvature, and tangential curvature (Zevenbergen & Thorne, 1987). Moreover, we derived the LS factor of the Universal Soil Loss Equation (USLE; Wischmeier & Smith, 1978) according to Moore et al. (1991). Finally, some topographic profiles were elaborated using the ArcMap 3D Analyst tools to investigate selected areas (*e.g.*, fluvial systems, slope breaks).

3.2.3. Inventory Map: mapping process

We produced an Inventory Map (IM) of sediment sources (Fig. 2) by integrating pre-existing inventories with field assessments, photointerpretation, terrain analysis, and manual digital-mapping. The Geomorphic Entities (GEs) were mapped at 1:5000 scale based on the identification of the primary morphogenesis (*i.e.*, gravitational, fluvial, runoff, litho-structural) contributing to the development of the geomorphic system. Moreover, superimposed geomorphic systems, related to different and chronologically differentiated morphogenetic settings, were mapped at the same scale (1:5000) using distinct overlaid GEs. The WGS84 – UTM 32N (EPSG: 32632) was used as the Reference Coordinate System.

The QD and IFFI databases were used as a starting point for the implementation of the IM. Their spatial accuracy and consistency were initially evaluated and validated. We made major improvements and corrections such as feature reclassification, redrawing, updating, and integration. Moreover, new features were extensively mapped by means of an integrated mapping process.

In particular, an extensive photo-interpretative analysis of recent orthophotos and Google® Earth 3D Imagery was carried out in combination with the visual interpretation of the hillshade relief map and the morphometric parameters. The analysis dealt with the identification of geomorphic and morphometric features, as well as different vegetation patterns highlighting the spatial extent of processes and landforms (Fig. 3). In some cases, the Technical Regional Map at 1:5000 scale (Regione Emilia-Romagna, 2020a) was used to interpretate orthophotos and satellite images. Geomorphological field surveys were carried out in selected test areas based on previous work by La Licata et al. (2023). The field-based characterization highlighted the interactions between different levels of processes contributing to landform development and sediment dynamics, on different spatio-temporal scales, within complex and polygenetic geomorphic systems (see Section 3.2.4).

Water erosion processes and related landforms were also extensively mapped. Rill-interrill erosion features were identified using various criteria such as (i) brightness of the soil due to the erosion of the dark organic topsoil horizon, (ii) specific rill structures visible in the orthophotos and/or satellite images, as well as (iii) susceptible morphological positions revealed by slope map and LS Factor (Maerker et al., 2020). In some cases, the NIR Orthophoto 2020 was used to identify erosion features in areas characterized by shrub and forest revegetation. We mapped fluvial erosion processes by identifying the main evidence of bank retreat and river-related slope erosion within the fluvial system. Finally, we identified litho-structural landforms as sediment sources if they are affected by other processes contributing to the sediment dynamics.

Additionally, we carried out an extensive multi-temporal photointerpretation over a 44-years period (La Licata et al., 2023), to investigate the past development of GEs over time, as well as their activity status (see Section 3.2.4).

3.2.4. Inventory Map: implementation and analysis of the database

The integrated database of the IM was set up in ArcMap (Fig. 2), following a hierarchical scheme as shown in Fig. 3. Initially, the Geomorphic Entities (GEs) mapped at 1:5000 according to the dominant morphogenetic processes were further characterized based on erosion and depositional dynamics. In particular, we followed the guidelines provided by the Italian Working Group for Geomorphological Mapping (Campobasso et al., 2021). The GEs were then subdivided and managed into distinct sub-databases based on the categories identified: (i) *Badlands and Gullies* (BG), (ii) *Rill-Interrill erosion* (RI), (iii) *Fluvial erosion* (BE), (iv) *Landslides* (LD), (v) *Litho-structural-erosional systems* (LR), (vi) *Slope deposits* (SD), and (vii) *Alluvial deposits* (AD). Subsequently, each vector object (*i.e.*, GE) has been characterized by attributes and further

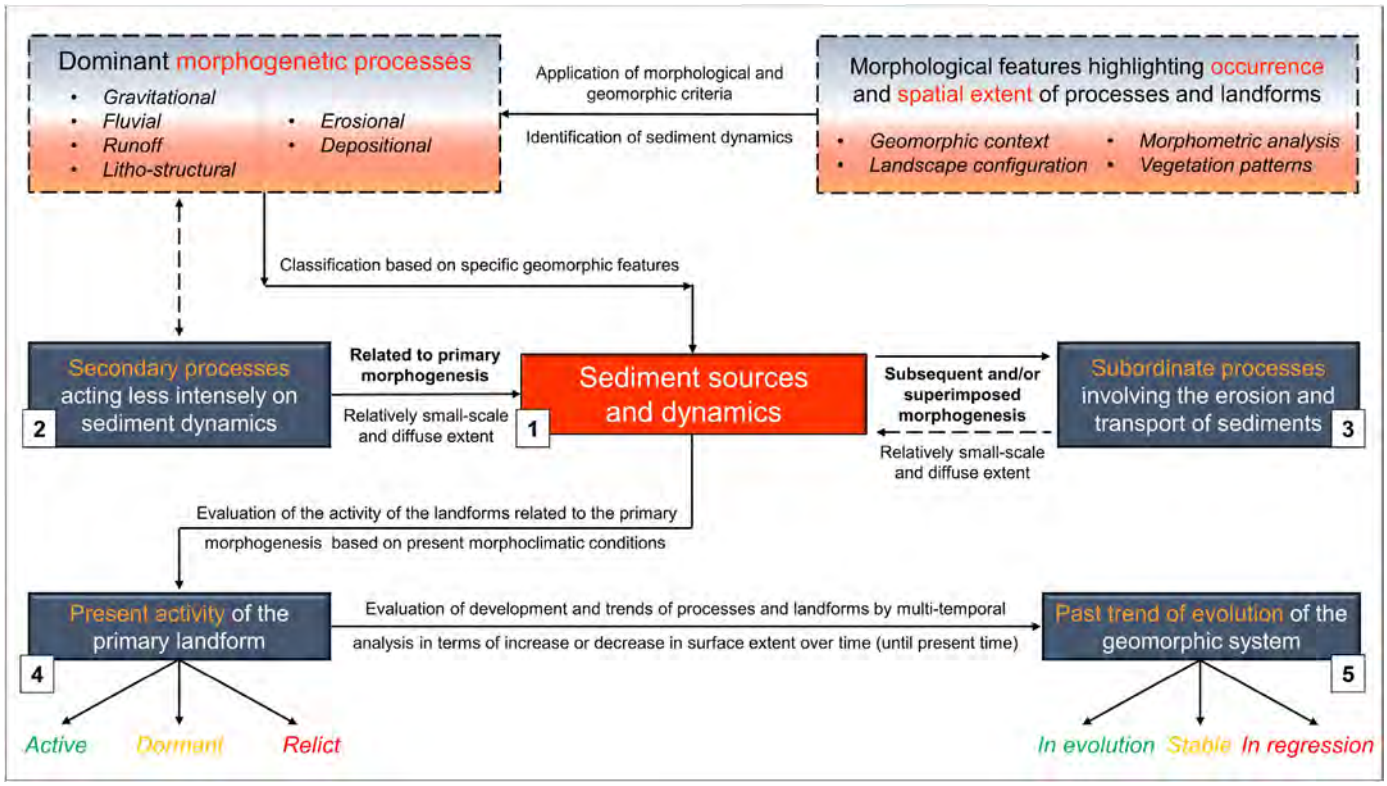

Fig. 3. Flowchart of the methodology used for the implementation of the Inventory Map database. The categorical variable n. 1, *i.e.*, *Sediment sources and dynamics*, is used as the reference variable.

categorized within the GIS database as shown in Fig. 3 (Steps 1–5):

1) *Sediment sources and dynamics* (surveyed at 1:5000 scale) (dp). Specific geomorphic characteristics allowing to uniquely classify the GEs as sediment sources (*e.g.*, badlands were distinct from isolated gullies, while landslides were classified based on type of movement; Trigila et al., 2010).
2) *Secondary processes* (surveyed at 1:2500 scale) (sp). Processes classified as secondary contributors to sediment dynamics, producing minor landforms related to primary morphogenesis (*e.g.*, piping affecting badland development). They are not always clearly recognizable in all the GEs of the same sediment source class and may have relatively less impact on sediment dynamics.
3) *Subordinate processes* (surveyed at 1:2500 scale) (cp). Processes related to the convergence of a subsequent and/or overlaid morphogenesis acting on the system, which involve erosion and transport dynamics (*e.g.*, erosion due to water runoff on landslide displaced material, or landsliding on badlands). They produce minor landforms related to different morphogenesis than the primary.

The categorization of 'secondary' and 'subordinate processes' depends mainly on their relative small-scale and diffuse extent that does not allow them to be mapped as individual GEs (*i.e.*, 1:5000 scale). Introducing these definitions is crucial for adequately acknowledging the presence of complex and polygenetic geomorphic systems as outlined by La Licata et al. (2023). This holds true even in cases where the limitations of the representation scale hinder detailed mapping.

4) *Present activity of the primary landform* (surveyed at 1:2500 scale) (ap). Landforms actively shaped by the primary morphogenetic agent or capable of reactivation under the current morphoclimatic conditions (*Active*) were distinguished from those no longer actively modelled by the primary morphogenetic agent or reactivatable in the current geomorphic and morphoclimatic setting (*Relict*) (Campobasso et al., 2021). Only for landslides, the *Dormant* class was introduced following SGSS (2005) and APAT (2007).
5) *Past trend of evolution of the geomorphic system* (surveyed at 1:2500 scale) (es). Processes and landforms whose development in terms of surface extent increased, stabilized, or decreased during a 44-years period were respectively classified as *In evolution*, *Stable*, or *In regression*. Anyway, a landform which is "in regression" is one whose extent decreased (*e.g.*, revegetation), despite the process which formed it might still occur in present time or the landform has a certain potential for reactivation. This trend is however referred to present time and it is not considered predictive.

Finally, spatial, geometrical and numerical analyses were performed on the sediment source classes (Fig. 3), with reference to their sub-database membership and the categorical variables 2, 3, 4, and 5.

3.2.5. Potential of Sediment Sources (PSS)

The Geomorphic Entities (GEs) were evaluated based on their potential for being sources of sediments, considering their attributes: (i) *Sediment sources and dynamics* (dp); (ii) *Secondary processes* (sp); (iii) *Subordinate processes* (cp); (iv) *Present activity of the*

primary landform (ap); (v) *Past trend of evolution of the geomorphic system* (es) (Fig. 4). The method adopted in this case study relies on an expert-based relative scoring system (Fig. 2 and Fig. 4), which qualitatively estimates the rating of the processes contributing to sediment dynamics in highly geomorphologically active areas in the Emilian Apennines (*i.e.*, based on the authors' knowledge and expertise, as well as on published literature; *e.g.*, Bertolini & Pizziolo, 2004; Bertolini et al., 2005; Staffilani et al., 2019; Coratza & Parenti, 2021; Pittau et al., 2021; La Licata et al., 2023).

Then, the GEs were assigned Provisional relative Scores (PSs) for the following variables: *dp*, *ap*, and *es*. PSs assigned to variables *dp*, *ap*, and *es* (*i.e.*, PS_dp, PS_ap, and PS_es) were estimated using a comparative process by which alternative categories of the same variable were qualitatively compared within a 'Versus Square Matrix Table' (VSMT). The VSMT allows to establish relative scores for different variables (Fig. 4). In particular, the VSMT was used to comparatively identify the potential of each GE in terms of severity or impact, based on different criteria: (i) geomorphic dynamic (PS_dp); (ii) process composition (PS_dp); (iii) the estimated mean tendency of processes to move sediments (PS_dp); (iv) activity of the landforms (*i.e.*, active landforms are supposed to have more potential than dormant and relict ones) (PS_ap); (v) evolution of the geomorphic system over time (*i.e.*, an increasing trend in surface extent is supposed to have more potential than stable or decreasing trends) (PS_es). Otherwise, Provisional relative Scores (PSs) for the variables *sp* and *cp* (*i.e.*, PS_sp and PS_cp) were set to 0 by default (*i.e.*, as to obtain the lowest assignable value in the next step). Afterwards, all the PSs were transformed according to Eq. (1) (Fig. 4):

$$FS_i = 1 + (PS_i / 2) \quad (1)$$

where *FS* is Final relative Score. That is, Eq. (1) represents a practical mathematical operation to obtain a continuous value distribution and to assign a value equal to 1 to all secondary (PS_sp) and subordinate processes (PS_cp), without discriminating them. *Relict* GEs were not considered in terms of FS_dp, FS_sp, and FS_es (differently than FS_cp) because they are preserved only as morphological features and are not directly involved in sediment dynamics (Campobasso et al., 2021).

The FSs of the different variables were subsequently summed to obtain a Total Score (Tot_score) calculated for each GE, denoting its overall potential contribution as a sediment source (Fig. 4).

Then, the channel network (CN) intersecting all sub-databases was extracted using ArcMap Geoprocessing tools. Each CN segment was automatically assigned a Tot_score equal to 1 (Fig. 4).

Therefore, the different sub-databases (*i.e.*, BG, RI, BE, LD, LR, SD, AD) and CN were rasterized using the SAGA GIS software (Fig. 4). Tot_scores were used as pixel values, while "no data values" were reclassified to 0.

Finally, the IM sub-databases and CN grids were integrated following Eq. (2) (see also Fig. 4):

$$PSS = (BG + RI + BE + LD + LR + SD + AD + CN) \times 10 \quad (2)$$

where PSS represents the *Potential of Sediment Sources* (Fig. 2). In particular, combining the raster layers of both the sub-databases and channel network, as given in Eq. (2), allows for the summation of the Tot_scores of overlapping GEs. Moreover, higher values are expected where the channel network segments intersect the GEs. Afterwards, the raster layers summation is multiplied by 10 to increase the weight and avoid decimal values.

3.2.6. Structural Sediment Connectivity (STC)

The DTM-based morphometric Index of Connectivity (IC) developed by Cavalli et al. (2013) was used to assess the structural

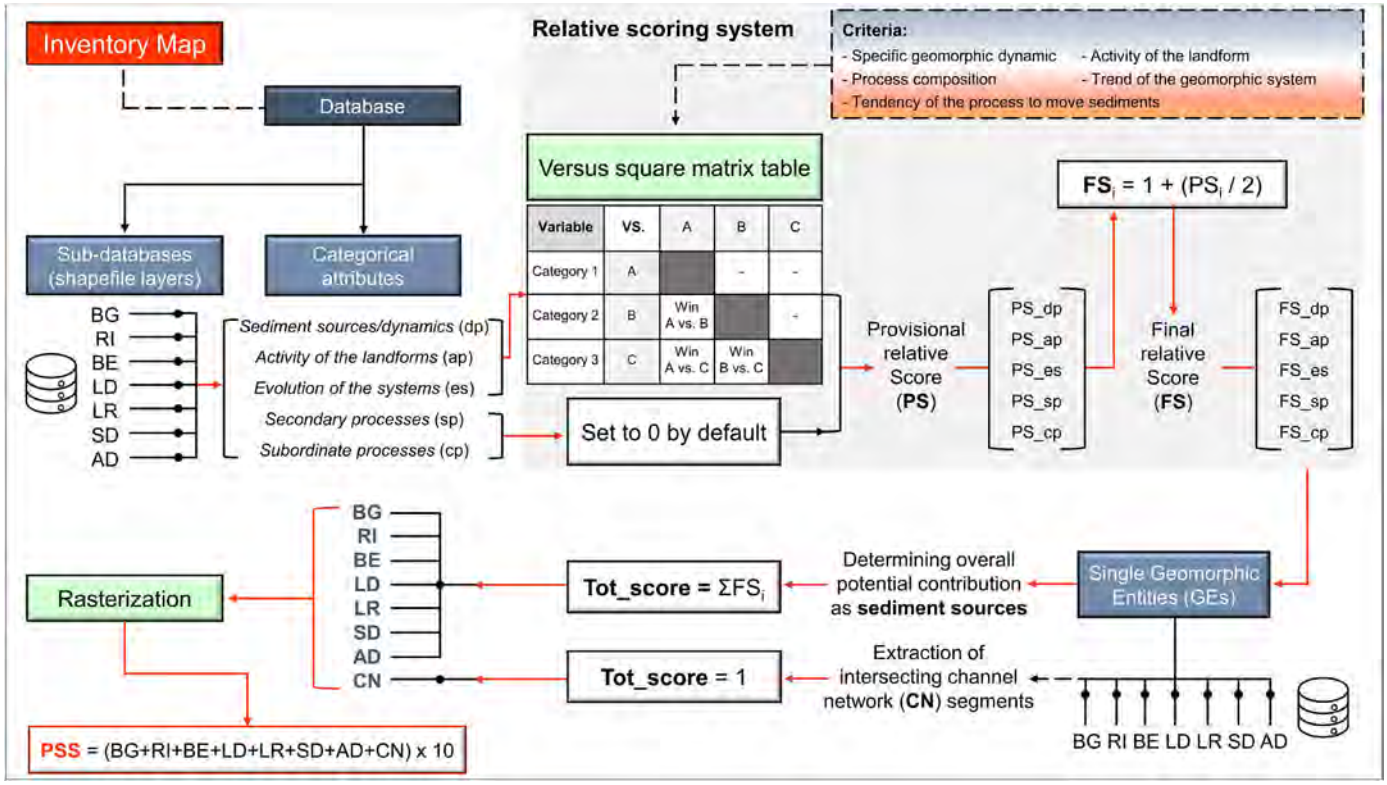

Fig. 4. Flowchart of the methodology used for the implementation of the *Potential of Sediment Sources* (PSS). The labels related to the Inventory Map sub-databases are the following: **BG**, *Badlands and Gullies*; **RI**, *Rill-Interrill erosion*; **BE**, *Fluvial erosion*; **LD**, *Landslides*; **LR**, *Litho-structural-erosional systems*; **SD**, *Slope deposits*; **AD**, *Alluvial deposits*.

sediment connectivity at the watershed scale (Fig. 2). The algorithm is based on the approach proposed by Borselli et al. (2008). We calculated for each raster cell the degree of linkage that controls sediment fluxes throughout the landscape, considering terrain attributes.

It is herein defined as:

$$IC = \log_{10}(D_{up} / D_{dn}) \quad (3)$$

where D_{up} and D_{dn} are defined by Eqs. (4) and (5) respectively (Table 1):

$$D_{up} = \overline{W}\,\overline{S}\sqrt{A_u} \quad (4)$$

$$D_{dn} = \sum_i \frac{d_i}{W_i S_i} \quad (5)$$

IC is defined in the range of [−∞, +∞], with connectivity increasing for larger values (Borselli et al., 2008; Cavalli et al., 2013).

The IC was computed using the stand-alone SedInConnect v. 2.3 software (Crema & Cavalli, 2018; Crema et al., 2015). The filtered and hydrologically corrected 5 m DTM was used as input data. Then, a 20 m buffer was applied to the DTM to avoid errors or approximations related to border effects (Cavalli et al., 2014). The main channel stems (*i.e.*, Lubiana creek and Arda river) and the Mignano reservoir (Fig. 1c) were used as target features. Small-scale sink features such as natural/artificial ponds and local depressions derived from the Technical Regional Map (1:5000) were introduced to decouple all sink draining areas from the connectivity assessment according to Cavalli et al. (2014). The regional land use map (*i.e.*, Land Use 2017, 1:10,000 scale; Regione Emilia-Romagna, 2020b) was used to derive the Manning's roughness coefficient (n). It was used to parameterize the weighting factor (W) of the IC (Bosino et al., 2022; Brardinoni et al., 2015; Persichillo et al., 2018) (Table 1). It represents a dimensionless proxy for impedance to water flow, with values varying according to different surface characteristics affecting roughness (Llena et al., 2019). We extracted Manning's n values of different land use classes from empirical tables following Goldin (2015) (Table 2). Finally, the weighting factor W was calculated using the following equation (Table 2):

$$W = 1 - n \quad (6)$$

The IC grid was normalized between 0 and 1, while decoupled areas upstream of the sinks were reclassified to 0. The normalized IC was used as a proxy for the *Structural Sediment Connectivity* (STC) component of the integrated model (Fig. 2).

3.2.7. Potential for Sediment Transport (PST)

According to Moore et al. (1991), we estimated the inherent physical potential for sediment delivery from slopes, based on the following equation:

$$A = R \times K \times LS \quad (7)$$

where A: annual average sediment delivery (Mg ha^{-1} yr^{-1}), R: annual average rainfall and runoff erosivity (MJ mm ha^{-1} h^{-1} yr^{-1}), K: soil erodibility (Mg h MJ^{-1} mm^{-1}), LS: slope length and slope steepness accounting for the effects of topography on erosion (dimensionless) (Fig. 2).

The R factor was used as an estimation of the annual average rainfall's kinetic energy and intensity and the rate of associated runoff. In this study we used the European rainfall erosivity dataset (500 m; Panagos et al., 2015a) provided by the European Soil Data Centre (https://esdac.jrc.ec.europa.eu; Panagos et al., 2022). The K factor represents an estimation of the susceptibility of sediments to erosion. It was derived from the regional soil erodibility dataset (20 m; Staffilani et al., 2019) provided by the GSSS-RER. The LS factor was calculated according to Moore et al. (1991) based on specific catchment area and slope to estimate the potential erosion at a point in the landscape, accounting for flow convergence and divergence and runoff energy (Moore & Nieber, 1989). Hence, the RKLS product represents the landscape capability to enable or facilitate sediment transport. In other words, it reflects the sediment transport occurrence depending on the surface runoff transport capacity and the availability of sediments to be transported.

Instead of the (R)USLE model (Panagos et al., 2015c; Renard et al., 1997), we explicitly omit the C factor as it is designed to specifically address the impact of land cover, crops, and crop management on rill-interrill erosion (Panagos et al., 2015b). Since most of the processes active within the study area are pouring out sediments into the channel network, our objective is to simulate the potential for sediment transport emphasizing the drainage system. Hence, we avoid including land use data in the modelling procedure. Furthermore, the impact of vegetation on sediment dynamics is already considered through the integration of the Manning's coefficient in the calculation of the STC. Additionally, according to Staffilani et al. (2019), local conservation strategies (P factor) were not considered in the equation as they are considered negligible in the study area.

According to Eq. (7), the R, K, and LS factors were then resampled at the same spatial extent to a resolution of 5 m using a B-Spline interpolation method. A maximum threshold corresponding to the 99.9th percentile was imposed to avoid model outliers. Finally, the resulting output (A) was normalized between 0 and 1 to obtain a relative measure of sediment transport. The normalized A was used as a proxy for the *Potential for Sediment Transport* (PST) component of the integrated model (Fig. 2).

3.2.8. Integrated assessment of potential hotspots of sediment sources and related dynamics

To combine geospatial geomorphological data (PSS) with structural sediment connectivity (STC) and potential for sediment

Table 1
Definition of the upslope (D_{up}) and downslope (D_{dn}) components of the IC model (from Cavalli et al., 2013).

Component	Equation	Variables	Definition
D_{up} (upslope)	4	$\overline{W}$ is the average weighting factor of the upslope contributing area $\bar{S}$ is the average slope gradient of the upslope contributing area (m/m) A_u is the upslope contributing area (m^2)	It represents the potential for downward routing of sediments available upstream depending on the upslope catchment area, mean slope, and a variable chosen as weighting factor.
D_{dn} (downslope)	5	d_i is the length of the flow path along the i^{th} cell according to the steepest downslope direction (m) W_i is the weighting factor of the i^{th} cell S_i is the slope gradient of the i^{th} cell (m/m)	It considers the flow path length through which a particle has to travel to reach the nearest target depending on the length of the path, the gradient along the downslope path, and a variable chosen as weighting factor.

Table 2
Manning's *n* overland flow roughness values assigned to each class of land use and the derived *W* factor. Manning's *n* are derived from Goldin (2015).

Land use class	Total area (ha)	Manning's *n* values	*W* factor
Arable lands	1561.75	0.200	0.800
Bare rocks	38.32	0.050	0.950
Industrial or commercial units	16.09	0.020	0.980
Infrastructures and services	11.90	0.020	0.980
Meadows	261.81	0.100	0.900
Mining areas, dumps, construction sites	12.37	0.010	0.990
Open spaces with scarce vegetation	94.38	0.150	0.850
Other agricultural areas	68.58	0.200	0.800
Road network	45.02	0.010	0.990
Shrub/herbaceous vegetation association	404.48	0.300	0.700
Urban fabric	221.72	0.020	0.980
Water bodies	75.95	0.001	0.999
Wetlands	62.58	0.001	0.999
Woods	5983.26	0.400	0.600

transport (PST), an integrated model was developed (Fig. 2):

$$HOTSED = [PSS \times (1 + PST)]^{STC} \quad (8)$$

where HOTSED stands for *Hotspots of sediment sources and related dynamics*.

In particular, the expression 1 + PST was used to upweight the pixel values of PSS based on environmental factors that contribute to the potential for sediment delivery. Specifically, PSS represents the sediments produced by the respective geomorphic processes, while PST depicts the transport capacity. Consequently, the coupled term of PSS and PST reflects the relative physical potential for sediment transport from specific sources. Additionally, the exponent STC, representing structural connectivity, is used to reduce the magnitude of morphometrically disconnected areas.

The HOTSED model was used to produce a map showing the location, extent, and distribution of *Hotspot areas of Sediment Sources and delivery* (HSS) (Fig. 2). All maps were displayed in the range of 2nd and 98th percentiles, providing a clearer view of the central tendency and pattern in the data while minimizing the impact of outliers.

Finally, HSS was classified into five classes of "relative hazard" (*i.e.*, *Very Low*, *Low*, *Medium*, *High*, *Very High*). The classification is based on the Jenks natural breaks method (Jenks, 1967), which was applied to values within the 2nd and 98th percentiles. The method minimizes the average deviation of each class from its own mean while maximizing the deviation of each class from the means of the other classes (Schneider et al., 2023). In addition, two further classes were added for pixel values equal to 0 (*i.e.*, *Non evaluable*) and 1 (*i.e.*, *Decoupled areas*). The classified HSS provides the *Hazard Map of Sediment Production and Delivery* (HPD) (Fig. 2).

We validated the consistency and accuracy of the model outputs through field-based observations in selected areas.

4. Results

4.1. Inventory Map (IM) of sediment-related landforms and processes

The mapping process led to the elaboration of the IM. It is subdivided in different sub-databases: *Badlands and Gullies* (BG), *Rill-Interrill erosion* (RI), *Fluvial erosion* (BE), *Landslides* (LD), *Litho-structural-erosional systems* (LR), *Slope deposits* (SD), and *Alluvial deposits* (AD).

The LD sub-database has been primarily implemented with data included in the IFFI Inventory (APAT, 2007). The latter has been improved by mapping recent landslide events and small-scale landslides below the detection mapping threshold. Moreover, landslides have been mapped in order to delimit also scarps and crowns. Landslides with a complex "style of activity" (*sensu* Cruden & Varnes, 1996) have been subdivided and reshaped in order to delimit the different types of movement (*i.e.*, mostly slides and flows). Flow landslides resulting from a complex landslide have been classified as 'earthflows' (see Bertolini et al., 2017) and distinguished from 'mudflows'. In some cases, new classes such as 'rock avalanches' (*sensu* Nicoletti & Sorriso-Valvo, 1991) have been introduced.

Moreover, SD and AD have been primarily implemented with data included in the QD Inventory (SGSS, 2005). GEs within SD and AD have been subsequently characterized based on depositional dynamic, geomorphic process, vegetation cover, and extent with respect to the morphological setting.

Areas affected by diffuse rill-interrill erosion forming the dominant morphogenetic process, on different land uses (*e.g.*, arable lands, meadows), have been mapped as GEs within RI, even when they are imposed on a landslide body stabilized by soil and vegetation cover. Otherwise, evidence of small-scale surficial erosion due to water runoff above the "fresh" landslide displaced material has been considered as a 'subordinate process' (*i.e.*, attribute) of GEs within LD (8.93% of the LD total number). Similarly, diffuse and small-scale shallow landsliding (*e.g.*, triggered by prolonged rill-interrill erosion, land use changes, or agricultural practices) has been considered as a 'subordinate process' of GEs within RI (5.59% of the RI area) rather than being mapped as a landslide process in LD. Within BG, isolated gullies have been distinguished from badlands. The latter are mapped as systems affected by a combination of multiple dominant (*i.e.*, rill-interrill and gully erosion), secondary (*i.e.*, piping), and/or subordinate (*i.e.*, landsliding) erosive processes. A total of 149 fluvial erosion source areas have been extensively identified along retreating banks within the main channels and mapped within BE.

Steep litho-structural rock walls (see La Licata et al., 2023) affected by diffuse and small-scale landsliding such as rock/debris falls (*i.e.*, dominant processes) have been mapped uniformly as polygenetic GEs in LR, without differentiating the specific landslide events. Particularly, all of the related GEs are also affected by water runoff (*i.e.*, subordinate processes), whereas only 62.36% of the LR area (25.07 ha) is affected by debris flows (*i.e.*, secondary processes) (Fig. 3).

Fig. 5a shows the main map that includes GEs grouped based on the sub-databases (Fig. 4) and classified based on the sediment sources (Fig. 3). The IM includes GEs covering a total of 4305 ha, that is, 48.92% of the total catchment area. The total area increases to 4640 ha if overlapping GEs are included. Considering the overall

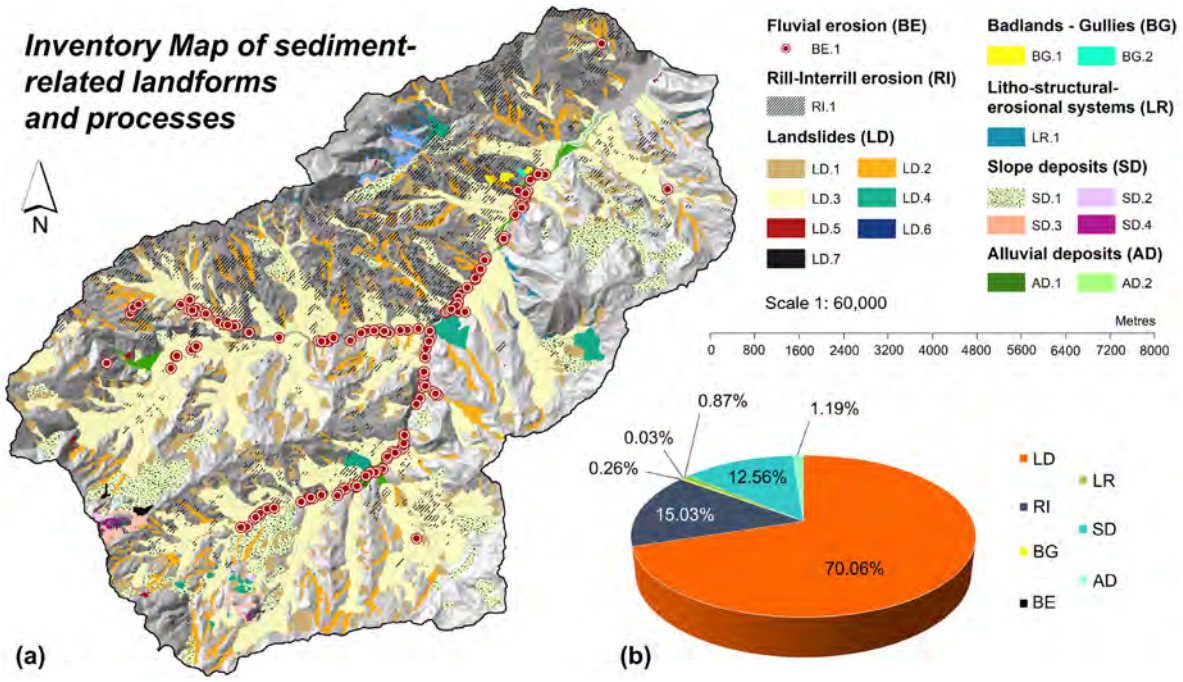

Fig. 5. (a) Inventory Map of Sediment-related landforms and processes of the upper Val d'Arda-Mignano watershed. Geomorphic Entities (GEs) are grouped based on the sub-databases: **BE**, *Fluvial erosion*; **RI**, *Rill-Interrill erosion*; **LD**, *Landslides*; **BG**, *Badlands and Gullies*; **LR**, *Litho-structural-erosional systems*; **SD**, *Slope deposits*; **AD**, *Alluvial deposits*. Then, GEs are classified based on *Sediment sources and dynamics* (see Fig. 3): **BE.1**, *Retreating banks*; **RI.1**, *Areas affected by rill-interrill erosion*; **LD.1**, *Roto-translational slides*; **LD.2**, *Slow mudflows*; **LD.3**, *Earthflows*; **LD.4**, *Block slides*; **LD.5**, *Rock/debris falls*; **LD.6**, *Debris flows*; **LD.7**, *Rock avalanches*; **BG.1**, *Badlands*; **BG.2**, *Isolated gullies*; **LR.1**, *Rock walls affected by diffuse rock/debris falls*; **SD.1**, *Gravitational/colluvial slope deposits s.l.*; **SD.2**, *Scree slopes*; **SD.3**, *Talus*; **SD.4**, *Eluvial deposits*; **AD.1**, *Fluvial terraces*; **AD.2**, *Floodplains*. BE.1 has been converted and displayed by point features for a better visual representation. (b) Percentage of the total area for each sub-database.

area, BG is 0.26%, RI is 15.03%, BE is 0.03%, LD is 70.06%, LR is 0.87%, SD is 12.56%, and AD is 1.19% (Fig. 5b). The results of the numerical, geometrical and statistical analyses of the database are reported in Appendix A.

4.2. Potential of Sediment Sources (PSS)

FS_dp has continuous values ranging from 1 to 6 (Table 3). The FS_ap values are distributed into 1 (*Relict*), 1.5 (*Dormant*), and 2 (*Active*) (Table 4). The FS_es values are distributed into 1 (*In regression*), 1.5 (*Stable*), and 2 (*In evolution*) (Table 5). The FSs for the variables *Secondary processes* (sp) and *Subordinate processes* (cp) are equal to 1. Only LD, SD, and AD have relict landforms. In this case, FS_dp, FS_es, and FS_sp have been set to 0, although the presence of subordinate processes increases the Tot_score in most of their GEs.

The range of resulted minimum and maximum Tot_scores in relation to the different sub-databases is: 8.5–13.5 for BG; 5–7 for RI; 9–10 for BE; 1–9.5 for LD; 8–10 for LR; 1–7 for SD; 1–5.5 for AD.

The PSS map provides initial information on where sediment-related landforms and processes are located and their relative potential as sediment sources (Fig. 6a). Its values range from 0 to 245,

Table 3
Versus square matrix table used to compare geomorphic processes linked to the categories of the variable *Sediment sources and dynamics* (dp) (Fig. 3 and Fig. 4). With reference to the classification into *Sediment sources and dynamics* (cfr. Fig. 5), all the *Slope deposits* are grouped under "Slope deposition", while the *Alluvial deposits* are grouped under "Fluvial deposition". Intersection cells represent the comparison of a certain category (row) to another (column), identified with unique code-letters. Each cell indicates which of the two categories being compared is evaluated to have a higher potential for sediment sourcing, in terms of severity or impact. PS_dp values are calculated by the sum of all the "wins". FS_dp values are calculated by applying Eq. (1).

Sediment sources and dynamics	VS.	A	B	C	D	E	F	G	H	I	L	M	PS_dp	FS_dp
Rill-interrill erosion	A												2.0	2.0
Gully erosion	B	B											9.0	5.5
Bank erosion	C	C	C										10.0	6.0
Roto-translational slide	D	D	B	C									7.0	4.5
Rock-debris falls	E	E	B	C	D								6.0	4.0
Debris flows	F	F	B	C	F	F							8.0	5.0
Slow mudflows	G	G	B	C	D	E	F						4.0	3.0
Block slides	H	H	B	C	D	E	F	G					3.0	2.5
Rock avalanches	I	I	B	C	D	E	F	I	I				5.0	3.5
Fluvial deposition	L	A	B	C	D	E	F	G	H	I			1.0	1.5
Slope deposition	M	A	B	C	D	E	F	G	H	I	L		0.0	1.0

Table 4
Versus square matrix table used to compare different categories of the variable *Present activity of the landform* (ap) (Fig. 3 and Fig. 4). Intersection cells represent the comparison of a certain category (row) to another (column), identified with unique code-letters. Each cell indicates which of the two categories being compared is evaluated to have a higher potential for sediment sourcing, in terms of severity or impact. PS_ap values are calculated by the sum of all the "wins". FS_ap values are calculated by applying Eq. (1).

Present activity of the landform	VS.	A	B	C	PS_ap	FS_ap
Active	A				2.0	2.0
Dormant	B	A			1.0	1.5
Relict	C	A	B		0.0	1.0

Table 5
Versus square matrix table used to compare different categories of the variable *Past trend of evolution of the geomorphic system* (es) (Fig. 3 and Fig. 4). Intersection cells represent the comparison of a certain category (row) to another (column), identified with unique code-letters. Each cell indicates which of the two categories being compared is evaluated to have a higher potential for sediment sourcing, in terms of severity or impact. PS_es values are calculated by the sum of all the "wins". FS_es values are calculated by applying Eq. (1).

Past trend of evolution of the system	VS.	A	B	C	PS_es	FS_es
In evolution	A				2.0	2.0
Stable	B	A			1.0	1.5
In regression	C	A	B		0.0	1.0

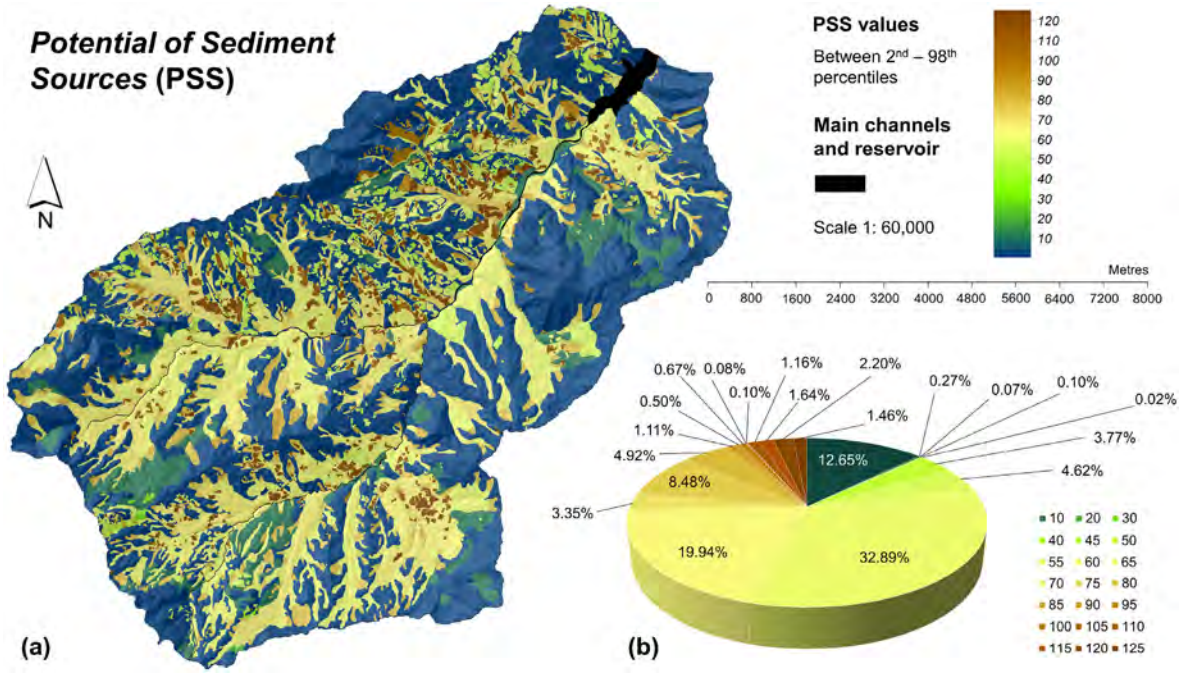

Fig. 6. (a) *Potential of Sediment Sources* (PSS) component used in the HOTSED model. The legend shows values (dimensionless) in the range of 2nd and 98th percentiles [10; 125]. Main channels and the reservoir are represented in black. (b) Percentage of all the values > 0 between the 2nd and 98th percentiles.

with higher values indicating a greater potential for sediment sourcing. The arithmetic mean is 32.13, while the standard deviation (STD) is 36.55. Values equal to 0 are 48.48% in terms of pixel distribution, indicating areas where no GEs were mapped (Fig. 5). Values > 0 amount to 51.52%. The range between the 2nd and 98th percentiles includes values from 10 to 125 (Fig. 6a), representing the central and more representative part of the full range distribution, with the most representative values of 60 and 65 (32.89% and 19.94% of the percentile range) (Fig. 6b). The latter values are essentially related to the wide extent of large-size dormant landslide bodies such as earthflows and block slides (Fig. 5a). Higher values (*i.e.*, 100–125) are mainly distributed on the left bank of the watershed (Fig. 6a), in areas where active processes with high potential occur (*e.g.*, bank erosion, debris flows), or where complex and polygenetic systems extend (*e.g.*, badlands, litho-structural-erosional landforms). Moreover, several GEs included in RI and BE overlap other sub-database grids, locally increasing the values of PSS (*e.g.*, rill-interrill erosion on stabilized landslide bodies, bank erosion at the landslide toe). The CN increases by 10 the overall value of GEs along the drainages that intersect them. Another representative value is 10 (12.65% of the percentile range; Fig. 6b), which is related to the extent of wide relict slope deposits in marginal areas or fluvial terraces near main channels (Fig. 5a).

4.3. Structural Sediment Connectivity (STC)

The STC provides a cell-based probability that sediments at a certain location of the watershed will arrive in the Lubiana creek, Arda river and Mignano reservoir by considering the small-scale hillslope morphometry (Fig. 7a). Its values comprise a full range from 0 to 1, with a mean value of 0.31 and a STD of 0.09 (Fig. 7b). The range between the 2nd and 98th percentiles includes values from 0.19 to 0.53 (Fig. 7a and b). Areas with higher STC values are distributed mainly next to the target features (Fig. 7a), indicating pixels where sediment is more likely to move throughout the landscape. Moreover, high values characterize also the dense hydrographic network that connects upper slope areas to the valley bottom (Fig. 7a), especially in the case of the main tributaries of the Lubiana creek and Arda river. However, the watershed is mostly characterized by low connected areas (Fig. 7a), suggesting locations where sediment is less subjected to transport towards the target features and, thus, where deposition is more probable. This is also revealed by the unimodal histogram distribution displaying a positive skewness, with a mode of 0.28 located below the mean (Fig. 7b). Fig. 7a also shows the presence of several decoupled areas draining to local sinks, which have been reclassified to 0.

4.4. Potential for Sediment Transport (PST)

The PST provides an estimate of the relative annual average amount of sediment potentially delivered from slopes (Fig. 8a). Its values comprise a full range from 0 to 1, with a mean of 0.10 and a STD of 0.10 (Fig. 8b). The range between the 2nd and 98th percentiles includes values from 0.01 to 0.41 (Fig. 8a and b). Areas with higher values correspond mainly to the dense network of tributaries of the Arda river and Lubiana creek, as well as along their banks, especially in the middle and upper part of the watershed (Fig. 8a). Moreover, Fig. 8a shows some cluster areas with high to very high values in localized parts of the watershed, due to a combination of high rainfall erosivity and high length-steepness. Open slopes composed of pelitic and chaotic units with moderate slope gradients are mainly characterized by intermediate values. However, the watershed is mostly characterized by low values, as revealed by the unimodal histogram distribution displaying a strongly positive skewness, with a mode of 0.05 located below the mean (Fig. 8b). Areas with very low values, mainly due to a combination of low soil erodibility and low slope length-steepness, are primarily located on the right side of the watershed (Fig. 8a).

4.5. The HOTSED model outputs

The HSS map provides the location of areas with a significant potential for both sediment sourcing and delivery (*i.e.*, hotspot areas; Fig. 9a), in terms of related geomorphic processes, their connectivity to the target features, and the potential for sediment transport. Its values range from 0 to 133.48, with a mean value of 2.20 and a STD of 2.88 (Fig. 9a and b). Values between the 2nd and 98th percentiles range from 0.26 to 9.68 (Fig. 9a and b). Areas with values of 0 (*i.e.*, dark blue areas; Fig. 9a) correspond to PSS values of 0 (Fig. 6a). Areas with values of 1 correspond to areas reclassified to

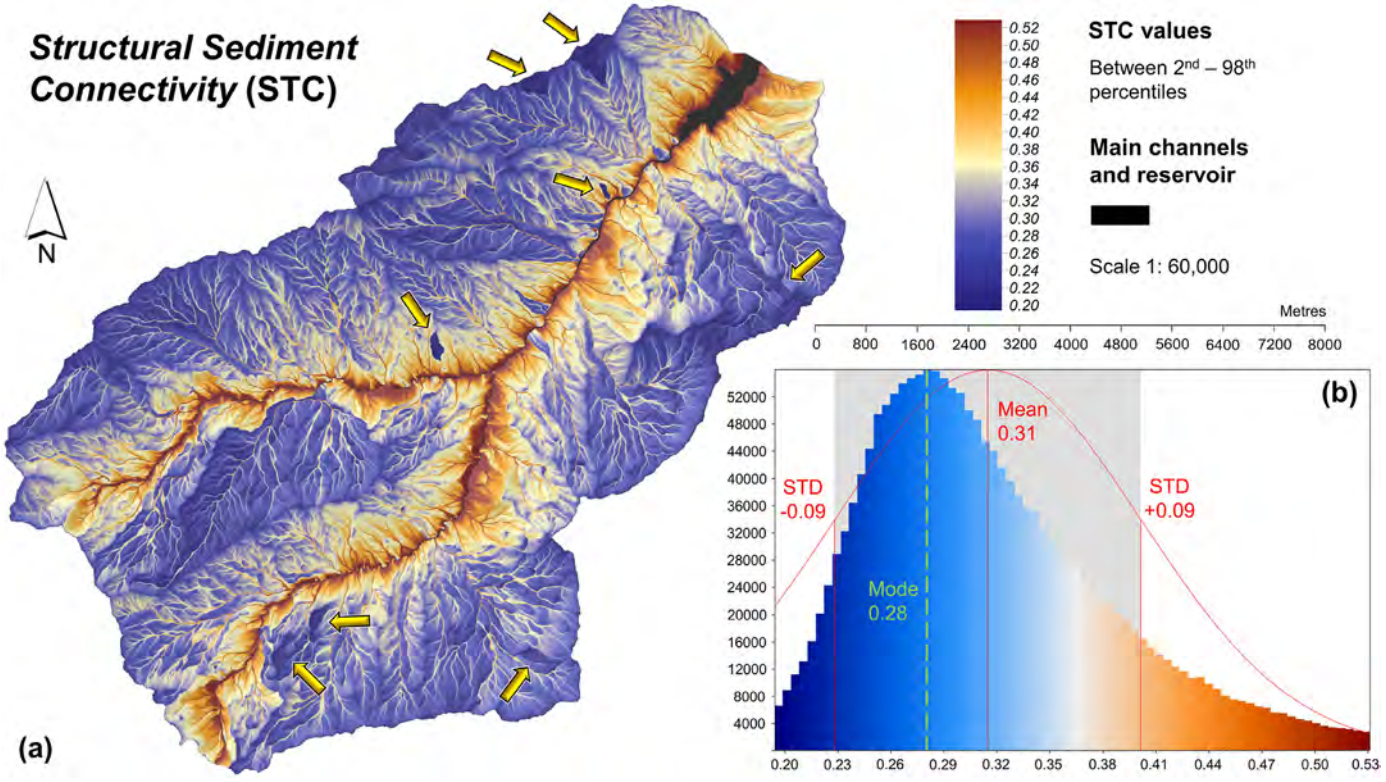

Fig. 7. (a) *Structural Sediment Connectivity* (STC) component used in the HOTSED model. The legend shows values (dimensionless) in the range of 2nd and 98th percentiles [0.19; 0.53]. Target features (*i.e.*, main channels and reservoir) are represented in black. Decoupled areas upstream of sink features are indicated with yellow arrows. (b) Histogram of STC values between 2nd and 98th percentiles, showing the deviation from the normal distribution. X axis: STC values; Y axis: number of pixels. The arithmetic mean ± STD (solid red lines) and the mode (dotted green line) are shown. The grey box shows values within the range of ±1 STD.

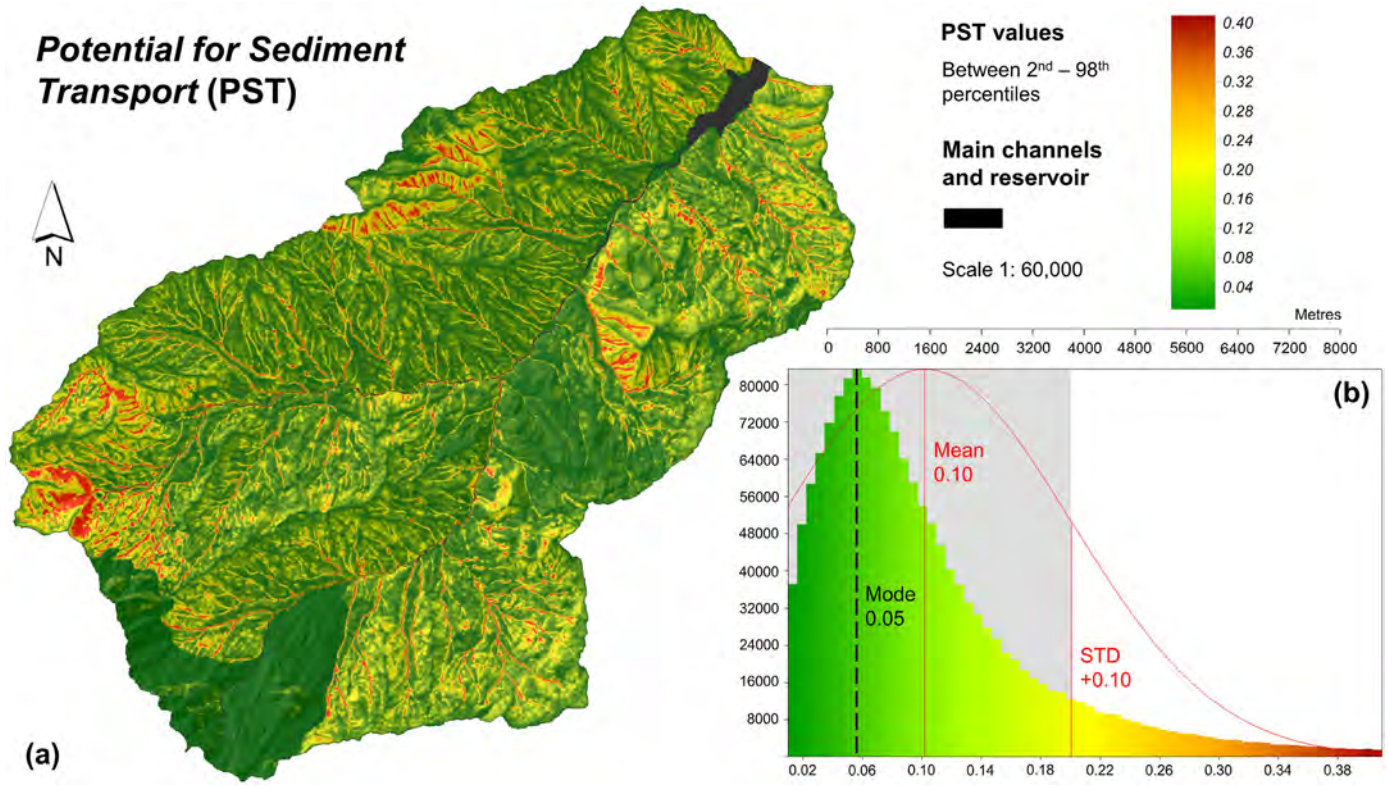

Fig. 8. (a) *Potential for Sediment Transport* (PST) component used in the HOTSED model. The legend shows values (dimensionless) in the range of 2nd and 98th percentiles [0.01; 0.41]. Main channels and the reservoir are represented in black. (b) Histogram of PST values between 2nd and 98th percentiles, showing the deviation from the normal distribution. X axis: PST values; Y axis: number of pixels. The arithmetic mean and the STD (solid red lines) and the mode (dotted black line) are shown. The grey box shows values from 0 to 1 STD.

0 in the STC (Fig. 7a). All of the PSS geomorphic features are now characterized with values > 1 (Fig. 9a).

Hotspot areas are mainly distributed upstream of the main channel stems (Fig. 9a). Areas displaying low to medium values are widespread in the watershed and are fully included within the range from 0 to 1 STD (Fig. 9b). These areas are located far from the main channel stems. However, the map emphasizes the presence of a dense drainage network that intersects geomorphic features, with values ranging from medium to high (Fig. 9a).

The histogram displays a multimodal pattern, with one isolated small peak at 1, a medium peak at the mode of 1.82, and a main peak at the main mode of 3.07 (Fig. 9b). Between the peaks at 1.82 and 3.07, the frequency decreases around the mean (Fig. 9b).

The classification of HSS provides an output (HPD) that depicts the potential of the landscape to produce and deliver sediments into the main channels and the reservoir, in terms of "relative hazard" (*i.e.*, changes in the physical system potentially affecting the environment and/or anthropic activities; Fig. 10a). Areas characterized by values equal to 0 are classified as *Non evaluable*, representing 47.88% of the total pixel distribution. Areas characterized by values equal to 1 are classified as *Decoupled*, representing 1.00%. Areas with values > 1 cover 51.12% and are distributed in five classes of relative hazard. Considering values > 1, the *Very High* class is the least representative (6.09%), mainly distributed close to the main channel stems or along the main tributaries (Fig. 10a and b). The *High* class covers 12.65%, which mostly connects areas with *Very High* and *Medium* hazard (Fig. 10a and b). The *Medium* class covers 26.88%, which is well distributed starting from higher classes close to the main channels, although several isolated upslope areas are included in it. Moreover, the drainage network intersecting areas included in the *Low* class is typically characterized by a *Medium* hazard (Fig. 10a and b). The *Low* class is the most representative within the watershed (39.86%; Fig. 10b). It comprises large and coalescent geomorphic systems distributed all over the watershed, especially in upslope areas (Fig. 10a). However, several areas adjoining the main channels are in the *Low* class (Fig. 10a). Finally, *Very Low* class is 14.52%, which is mainly distributed in few clusters especially in upslope or marginal areas (Fig. 10a).

A validation procedure based on the comparison of model inputs/outputs, along with illustrative field-based observations, is reported in Appendix C (Figs. C.1, C.2, C.3, and C.4).

5. Discussion

We developed an integrated model (HOTSED) that covers static geospatial information on: (i) sediment-related landforms and processes (Fig. 5) and their potential as sediment sources (Fig. 6), (ii) the landscape capability to facilitate sediment transport based on topography, flow pathways, and channel network (Fig. 7), and (iii) the potential for sediment transport from hillslopes (Fig. 8). HOTSED assesses where and to what extent landscape has the highest potential to produce sediment and deliver it considering the main channels and the reservoir as target features, as well as where landscape is more predisposed to store sediments. Unlike other approaches that deal with different formats and structures of data that are often difficult to join and interpret, HOTSED is a raster-based model that provides a holistic approach allowing to detect emergent properties of the system within a unique, intuitive and

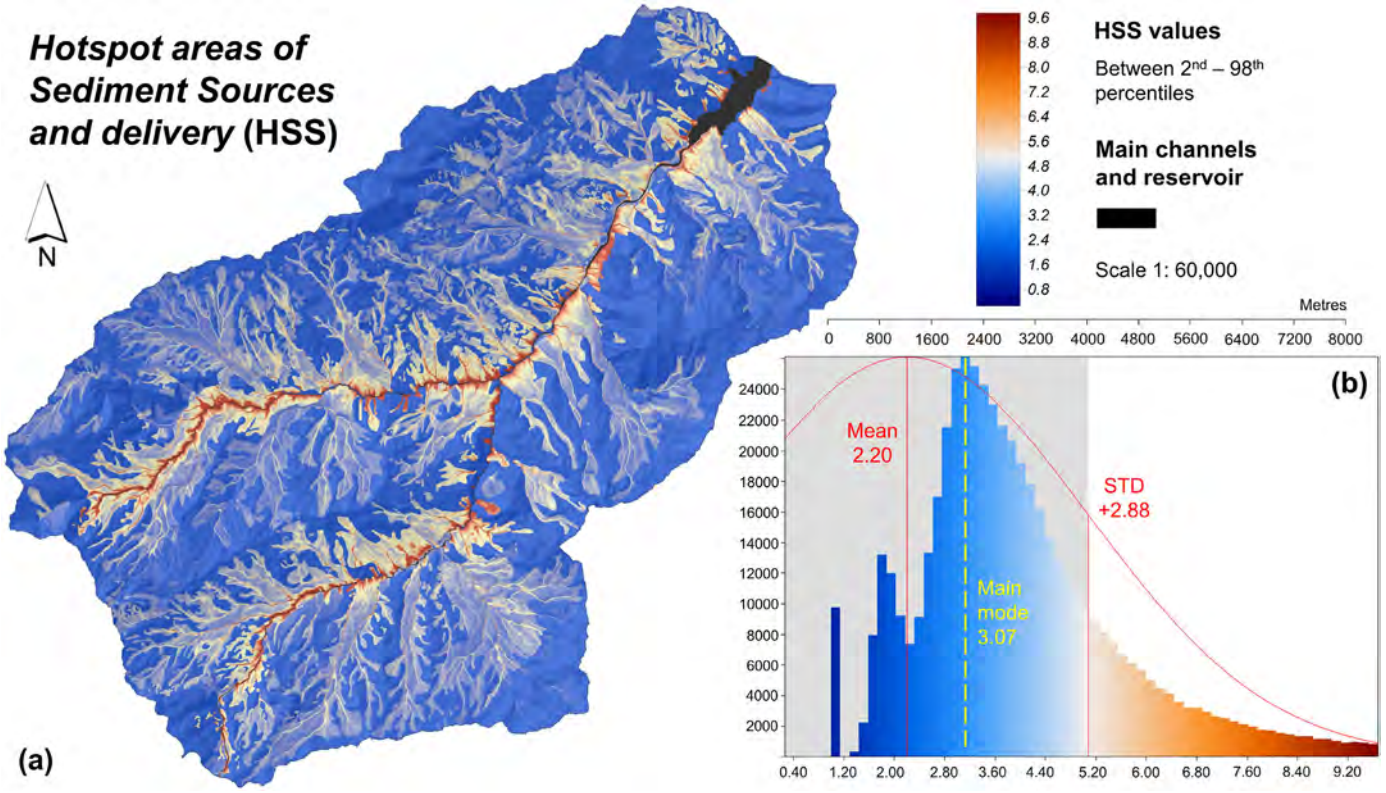

Fig. 9. (a) *Hotspot areas of Sediment Sources and delivery* (HSS) derived from the HOTSED model. The legend shows values (dimensionless) in the range of 2nd and 98th percentiles [0.26; 9.68]. Main channels and the reservoir are represented in black. (b) Histogram of the HOTSED values between 2nd and 98th percentiles, showing the deviation from the normal distribution. X axis: HSS values; Y axis: number of pixels. The arithmetic mean and the STD (solid red lines), and the main mode (dotted green line) are shown. The grey box shows values from 0 to 1 STD.

comprehensive output (Fig. 9 and Fig. 10).

Fig. 9 shows the distribution of the hotspots of sediment sources within the upper Val d'Arda. They are distributed mainly in areas adjoining the main channels or upstream of the reservoir. The presence of "very high" relative hazard values in localized areas may have multiple geomorphological significance. It might imply that certain specific topographic features such as proximity to the target features or hillslope position could have determined high STC (Fig. 7 and Fig. C.1) and PST (Fig. 8) values respectively. However, geomorphic features with a high potential are particularly frequent in these areas (Fig. 6). Indeed, this hazard class includes several small-to medium-size active landslides (Fig. 5), often affected by erosion due to water runoff, as well as the most distal part of some large earthflow toes, especially where fluvial erosion occurs (Fig. 5 and Fig. C.1; de Vente et al., 2006; Pittau et al., 2021). Most of these landslides are active and display evidence of (re) activation within the last ~50 years, pouring out sediments into the channels with a high degree of linkage from source to sink. Furthermore, the location, distribution, and extent of large landslides like earthflows (Fig. 5), compared to STC and PST outputs (Fig. 7 and Fig. 8), revealed that the degree of physical and functional linkage between different landscape units is largely affected by these geomorphic features. Thus, large landslide bodies are expected to affect the spatial arrangement of hydro-geomorphic processes, which in turn control the transfer of sediments within the watershed (Bracken et al., 2013; Wainwright et al., 2011). Most of drainages flowing alongside the main landslide bodies, as well as those intersecting them, can be considered as stream corridor sediment sources (Gellis et al., 2016; Gellis & Walling, 2011), locally acting as linear hotspots (Fig. 9 and Fig. C.2). This is mainly due to the high STC and PST values characterizing the main channel tributaries (Figs. 7, 8 and Fig. C.2), as well as to the high PSS values (Fig. 6) resulting from the sum of CN and LD Tot_scores (Fig. 4). Moreover, the model is capable of highlighting a localized increase in HSS values in some geomorphic systems such as rock walls affected by diffuse landsliding (*i.e.*, LR.1), along drainages that were not directly emphasized in PSS, mainly due to increasing values in STC and PST. In some cases, field-observations revealed that this increase perfectly matches the occurrence of debris flows (*i.e.*, 'secondary processes' of LR.1) (Fig. C.3).

Badlands are complex and polygenetic geomorphic systems (Battaglia et al., 2002; La Licata et al., 2023) displaying a high potential contribution in terms of sediment production and export in the study area (Bosino et al., 2019, 2022; Castaldi & Chiocchini, 2012; Poesen et al., 2003). Nevertheless, despite badlands have a similar high potential as sediment sources and for sediment transport along their drainages, their geomorphic hazard (Fig. 10) mainly depends on their distance from the target features used to compute the STC. This means that structural connectivity plays a major role in determining the potential contribution in the delivery of sediments produced by these sources.

Moreover, the IM highlights the presence of several depositional landforms such as slope deposits and alluvial deposits associated with fluvial terraces (Fig. 5). As previously highlighted by La Licata et al. (2023), these features are capable of storing sediments over various spatio-temporal scales as sediment sinks (Gellis et al.,

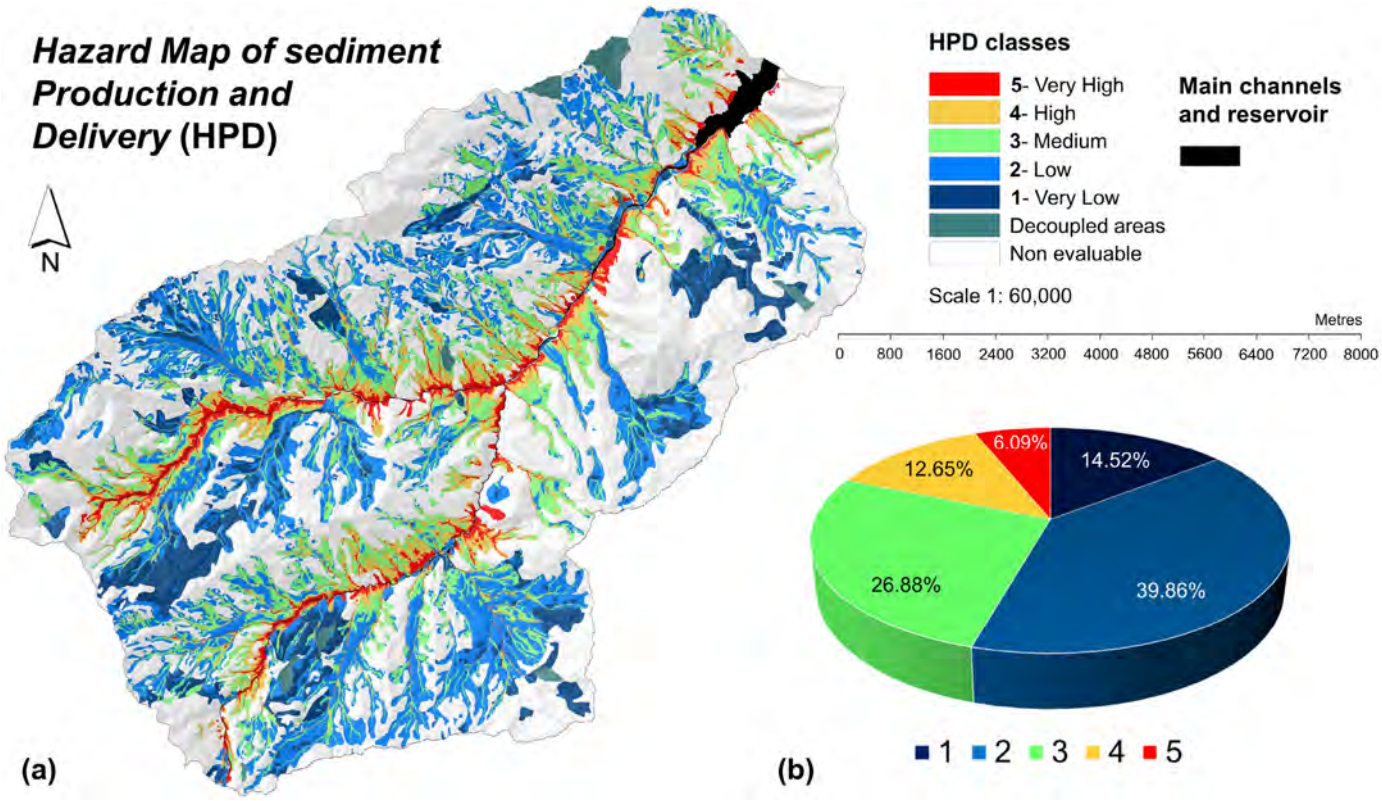

Fig. 10. (a) *Hazard Map of sediment Production and Delivery* (HPD) derived from the HOTSED model. The legend shows different classes of relative hazard (1 - *Very Low*, 2 - *Low*, 3 - *Medium*, 4 - *High*, 5 - *Very High*) based on the Jenks natural breaks method applied to values comprised in the range of 2nd and 98th percentiles [0.26; 9.68]. Values equal to 0 and 1 are classified, respectively, as "Non evaluable" and "Decoupled areas". Main channels and the reservoir are represented in black. (b) Percentage of the different classes of relative hazard.

2016), based on a low geomorphic potential in delivering sediment downstream (as they are mostly relict features) and a low sediment connectivity (Fig. C.3). In particular, the HSS and HPD maps efficiently depict these particular morphological and geomorphic settings, which are distributed in areas with "very low" relative hazard (Fig. 9 and Fig. 10). As stated by Turley and Hassan (2023), these areas may be considered as a physical representation of disconnectivity in the landscape, being geomorphic buffers that prevent sediment from entering the channel and reaching the catchment outlet (*sensu* Fryirs et al., 2007; Fryirs, 2013). Furthermore, the histogram distribution of STC (Fig. 7b) suggests that a large amount of sediments could be stored in restricted areas within the watershed, where sediment transport and redistribution are more difficult. Hence, these findings may suggest that the upper Val d'Arda has a low sensitivity to external impacts due to the attenuation of sediment fluxes reaching the catchment outlet, thus being out of equilibrium (*i.e.*, the input into the system is not equal to the system output; Hoffmann, 2015). On the other hand, it is noteworthy that these landforms may supply sediments to the drainage system if subordinate erosive processes affect them (Gellis et al., 2016). Nevertheless, field-observations support the hypothesis that a general attenuation is, to some extent, controlled also by small features like ponds and local depressions, which disconnect small portions of the catchment area (Fig. C.4).

Other important sediment storages in the watershed are large landslide bodies such as earthflows, block slides, and mudflows (Fig. 5). However, unlike slope and fluvial deposits, the latter are not relict landforms (Campobasso et al., 2021), as they typically exhibit very slow and intermittent movements that persist for long periods (Bertolini et al., 2017; Bertolini & Pizziolo, 2008), alternating with more rapid "surges" (Hungr et al., 2014). Some authors have already focused on the role of slow-moving earthflows as primary sources that supply sediment to the river network in the Northern Apennines (Simoni et al., 2013), especially when combined with other processes (*e.g.*, bank erosion; La Licata et al., 2023). Even in this case, the HSS and HPD maps represent efficiently their potential contribution to sediment sourcing and delivery (Fig. 9 and Fig. 10). They are characterized on average by low values while showing increasing hazard where other processes and dynamics interact with them influencing their sediment supply, as well as where intrinsic properties of the system increase their predisposition to act as sediment sources (Fig. C.1 and C.2).

Therefore, we argue that highlighting the location and extent of sediment storages within the watershed is crucial for understanding the spatial and temporal patterns of sediment movement, as well as the overall efficiency of sediment transfer between different parts of the landscape (see also Turley & Hassan, 2023). Moreover, understanding the controls of connectivity is vital to predict how the system could be modified due to climatic and socio-economic changes (Hoffmann, 2015).

Consistent with the conceptual model of the catchment-scale connectivity proposed by Heckmann et al. (2018), the HOTSED model integrates different environmental variables representing external forcings and intrinsic properties of the system. In this

context, the rainfall erosivity represents the main hydrological driver of sediment (re)mobilization and water/sediment fluxes. Differently, upslope contributing area, specific catchment area, slope gradient, flow convergence and divergence, length of the flow paths, vegetation roughness, and soil erodibility account for both structural and functional intrinsic properties of the system. Furthermore, the location of sediment sources relative to the channel network adds to the list of the connectivity-related properties of the watershed (Heckmann et al., 2018). Moreover, as strongly recommended by previous authors (*e.g.*, Martini et al., 2022), in our study the assessment of sediment connectivity has not been considered as the ultimate outcome of the research, but as a tool for predicting the contribution of sediment sources based on their geomorphic potential.

According to other authors, combining the static geomorphic potential of the landscape with the relative efficiency of sediment transfer between specific sources and sinks (Wainwright et al., 2011) represents an effective approach to characterize the variability of both structural and functional properties of the connectivity (Mahoney et al., 2021). Moreover, our approach provides a catchment-scale assessment of the process-based potential of the system to supply sediments. This potential is weighted according to both the availability and accessibility of sediments (see also Najafi et al., 2021b), as it accounts for sediment storage, remobilization and redistribution throughout the landscape. Thus, external drivers and system properties directly or indirectly influence geomorphic processes, which in turn govern the transfer of water and sediment across the landscape (Heckmann et al., 2018). Therefore, our model implements the concept of 'process-based connectivity', which was introduced by Bracken et al. (2013) to convey how spatial patterns of watershed characteristics interact with processes to produce connected flow and, hence, water and sediment transfer. Therefore, HOTSED evaluates functional connectivity as an emergent property of the system resulting from the integration of geomorphological spatial data and the spatial distribution of watershed characteristics.

However, Bracken et al. (2015) defined functional connectivity as the actual transfer of sediment considering the time component and the frequency–magnitude distribution of sediment detachments. Integrating this definition into our model is challenging due to the highly heterogeneous nature of time, frequency, and magnitude variables in an approach that encompasses all the processes contributing to sediment dynamics. Indeed, the processes occurring within the upper Val d'Arda operate at quite different spatial and temporal scales with respect to the sediment delivery in fluvial system (Fryirs et al., 2007; Harvey, 2002; Turley & Hassan, 2023). For instance, landslides have been shown to exhibit a high variability of morphology, extent, distribution, magnitude, and frequency. Thus, they are not easily comparable to each other in terms of sediment delivery. Even more their comparison with different morphogenetic processes is difficult, especially considering geomorphic systems coevolving with human activities (La Licata et al., 2023). For instance, rill-interrill erosion typically shows a high temporal variability. It is particularly frequent on arable lands, as soil is easily eroded from bare and disturbed soil surfaces (Montgomery, 2007). Consequently, its impact is influenced by normal annual or seasonal tillage operations (Angileri et al., 2016; García-Orenes et al., 2012). This is expected to affect also the temporal variability of sediment export (Lizaga et al., 2020). This evidence suggests that the season or a particular time of the year is important with respect to certain sediment sources (Gellis et al., 2016). Moreover, La Licata et al. (2023) pointed out that in the study area a single geomorphic system might imply both transfer and depositional dynamics, involving multiple and subordinate processes producing complex and polygenetic systems. Consequently, a raster-based sum of overlaying processes that represents the static geomorphic potential of the landscape, as proposed in the present study, is believed to be an effective method for dealing with geomorphologically highly heterogeneous watersheds. Moreover, our approach is not designed to deal with future geomorphic system evolution (*e.g.*, driven by storm events or seasonality) as it does not account for variations in spatial distribution and extent of Geomorphic Entities. However, such variations can be addressed by comparing model outputs derived through the compilation/updating of sediment source inventories after specific climatic events or periods. Anyway, Cho et al. (2023) pointed out that hydrological processes through different pathways and timing may have different effects on sediment connectivity, as they are affected differentially by rainfall duration, magnitude and frequency. That is, hydrological processes may activate different sediment sources, storage areas, and transit pathways based on different storm events (Cho et al., 2023). For this reason, an approach that considers the potential for sediment transport according to annual average conditions (*i.e.*, rainfall erosivity, land use) might provide a more convenient and accessible tool for identifying hotspot areas of sediment dynamics within a watershed management framework.

Zingaro et al. (2019) proposed a sediment flow connectivity approach (SCI) based on a gradient-based flow accumulation algorithm weighted by a sediment mobility index. It expresses the potential availability of detachable sediment as a result of external forcings and landscape characteristics, as well as of sediment connectivity in the catchment. However, despite the fact that the SCI index is able to represent both lateral and longitudinal sediment pathways within the system, it is not designed to account for upslope sediment sources nor for the processes that are actually moving sediments within channels (Zingaro et al., 2019). In contrast, HOTSED provides an assessment of the static landscape potential for sediment sourcing and delivery after various geomorphic processes have occurred, without considering the dynamic aspect of sediment routing. Nonetheless, our approach should not be considered as an endpoint, but rather as a starting tool for future implementation, both in a scientific and watershed management perspective. The incorporation of a hydrological model into the HOTSED methodological framework might provide actual water and sediment flows, improving the assessment of sediment sourcing and supply (Hooke & Souza, 2021). Moreover, integrating hydrological modelling is necessary to account for variations between different rainfall events/periods (*e.g.*, López-Vicente & Ben-Salem, 2019), as well as to investigate system response to climate changes (Li & Fang, 2016). Additionally, the integration of slope stability/susceptibility models is needed to properly assess sediment dynamics driven by slope failures (Cislaghi & Bischetti, 2019).

The approach proposed in this paper can be considered simple and replicable in several different contexts. Its reproducibility relies mainly on the ever-increasing availability of geospatial technologies such as GIS-based applications, as well as the growing availability and quality of DTMs (Bishop et al., 2012; Heckmann et al., 2018). Furthermore, the increasing availability of geomorphological spatial data usually provided by national or regional authorities, which can be supplemented using GIS applications and/or digital mapping, allows for an assessment of the distribution and characteristics of sediment sources, even in remote or challenging

areas. Nevertheless, despite a detailed mapping approach usually provides a higher accuracy in representing geomorphic features and related dynamics, especially in geomorphologically highly active areas, it is generally considered a time-consuming method and however limited to smaller basins (Wichmann et al., 2009). An alternative could be the derivation of information from remote sensing and terrain analysis by partitioning the watershed into Geomorphic Process Units (GPUs) or Erosion Response Units (ERUs) having the same spectrum of processes, as proposed by Gude et al. (2002), Bartsch et al. (2002), or Maerker et al. (2001). Moreover, it is worth noting that the application of the HOTSED model in other morphoclimatic environments (*e.g.*, European Alps) might make it necessary to revise and adapt the scores used to weight the different processes (see Table 3), thus creating *ad hoc* comparative matrix tables.

6. Conclusion

We presented a novel methodology to integrate geospatial information of sediment sources and related dynamics with the assessment of structural and functional properties of the connectivity. In particular, we developed a new GIS-based integrated model named HOTSED, which is designed to assess where and to what extent landscapes have the potential to produce sediment and to transport it, as well as where landscapes are more predisposed to store sediments.

We tested our approach in the upper Val d'Arda-Mignano watershed (Northern Apennines, Italy), starting from the elaboration of a comprehensive Inventory Map (IM) of sediment sources, along with its spatial, numerical, and geometrical analysis. Furthermore, we used IM-derived data to estimate the geomorphic *Potential of Sediment Sources* (PSS) adopting a relative scoring system. Moreover, proxies for *Structural Sediment Connectivity* (STC) and *Potential for Sediment Transport* (PST) were computed combining both structural and functional intrinsic properties of the system. Afterwards, the integration of PSS, STC, and PST was achieved through a raster-based calculation method, which resulted in the HOTSED model.

HOTSED provides a holistic methodology capable of revealing emergent properties of the system through a single, intuitive, and comprehensive raster output. Our methodology has proven to be particularly effective in geomorphologically highly active Mediterranean areas, especially where different processes may combine and/or overlap to each other producing complex and polygenetic geomorphic systems. Therefore, our study contributes to a deeper understanding of the differential contribution of geomorphic processes to sediment dynamics in general, and particularly in the Northern Apennines (Italy).

Nonetheless, our study is extending beyond its scientific relevance, providing a valuable tool for local authorities. HOTSED provides the methodological framework to support management decisions regarding the identification of major hillslope sediment source areas within the upper Val d'Arda and, thus, the proposal of new strategies for limiting sedimentation in the reservoir (*e.g.*, mitigation measures, short- and long-term monitoring).

Further improvements may enhance the performance of the model. For instance, continuous C factor values obtained from Normalized Difference Vegetation Index (NDVI) remote sensing imagery may be used as a weighting factor for the computation of STC, thus yielding a more realistic vegetation distribution along with their impact influencing sediment fluxes. Moreover, in the current stage of development, the HOTSED framework represents the average conditions of the watershed as it integrates a static representation of the extent and distribution of sediment sources and land cover, as well as a rainfall erosivity index at the annual scale. However, monthly and seasonal data on NDVI and rainfall erosivity might be used to assess variations in vegetation impedance to water flows and potential for sediment transport over the year. Additionally, the comparison between past, present and future rainfall erosivity, as well as for land use, might provide insights into the sensitivity of the system to climatic and land use changes. Finally, the model could be further validated by means of sediment fingerprinting techniques.

CRediT authorship contribution statement

Manuel La Licata: Writing – review & editing, Writing – original draft, Visualization, Software, Methodology, Investigation, Formal analysis, Data curation, Conceptualization. **Alberto Bosino:** Writing – review & editing, Investigation, Conceptualization. **Seyed Hamidreza Sadeghi:** Writing – review & editing, Conceptualization. **Mattia De Amicis:** Software, Resources. **Andrea Mandarino:** Writing – review & editing. **Andrea Terret:** Resources. **Michael Maerker:** Writing – review & editing, Supervision, Project administration, Investigation, Funding acquisition, Conceptualization.

Declaration of competing interest

The authors declare that they have no known competing financial interests or personal relationships that could have appeared to influence the work reported in this paper.

Acknowledgments

This research was conducted with the financial support of the Earth and Environmental Sciences PhD-PON program (Research & Innovation, 2014–2020, *Education and research for recovery - REACT-EU*, DOT1322534-4) of University of Pavia, Department of Earth and Environmental Sciences. This research was also conducted with the financial support of the RTDA-PON program (Research & Innovation 2014–2020, *Education and research for recovery - REACT-EU,* C6-G-32370-3), University of Milano-Bicocca, Department of Earth and Environmental Sciences. We were also supported by the Belmont ABRESO project (https://www.belmontforum.org). We would like to thank the Italian Ministry of University and Research for funding the PRIN project 2022C2XPK7 entitled: "Full cOveRage, Multi-scAle and multi-sensor geomorphological map: a practical tool for TerrItOrial plaNning - FORMATION". The present research also benefited from the collaboration with Geoscape Soc. Coop. (https://www.geoscape.it), partner of the PhD Project n. F11B21008530007 (M. La Licata). We also thank the staff of Consorzio di Bonifica di Piacenza (https://www.cbpiacenza.it) for the valuable support during the field surveys.

Appendix A

Table A.1

Numerical, geometrical and relative frequency outputs of the Inventory Map (IM) database analysis. The second row reports the sub-databases: **BG**, *Badlands and Gullies*; **RI**, *Rill-Interrill erosion*; **BE**, *Fluvial erosion*; **LD**, *Landslides*; **LR**, *Litho-structural-erosional systems*; **SD**, *Slope deposits*; **AD**, *Alluvial deposits.* The third row reports the sediment sources/dynamics classes: **BE.1**, *Retreating banks*; **RI.1**, *Areas affected by rill-interrill erosion*; **LD.1**, *Roto-translational slides*; **LD.2**, *Slow mudflows*; **LD.3**, *Earthflows*; **LD.4**, *Block slides*; **LD.5**, *Rock/debris falls*; **LD.6**, *Debris flows*; **LD.7**, *Rock avalanches*; **BG.1**, *Badlands*; **BG.2**, *Isolated gullies*; **LR.1**, *Rock walls affected by diffuse rock/debris falls*; **SD.1**, *Gravitational/colluvial slope deposits s.l.*; **SD.2**, *Scree slopes*; **SD.3**, *Talus*; **SD.4**, *Eluvial deposits*; **AD.1**, *Fluvial terraces*; **AD.2**, *Floodplains* (Fig. 5). Units: n. = number; %* = percentage related to the sub-database membership; %** = percentage related to the IM total for that category; ha = hectares.

Database																											IM
Sub-databases		BG			RI		BE		LD								LR		SD					AD			
Sediment sources		BG.1	BG.2	Tot.	RI.1	Tot.	BE.1	Tot.	LD.1	LD.2	LD.3	LD.4	LD.5	LD.6	LD.7	Tot.	LR.1	Tot.	SD.1	SD.2	SD.3	SD.4	Tot.	AD.1	AD.2	Tot.	Total
Number of GEs	n.	12	7	19	1432	1432	149	149	519	222	142	25	11	5	3	927	47	47	50	5	31	7	93	16	4	20	**2687**
	%*	63.16	36.84	100.00	100.00	100.00	100.00	100.00	55.98	23.95	15.32	2.70	1.19	0.54	0.32	100.00	100.00	100.00	53.76	5.38	33.33	7.53	100.00	80.00	20.00	100.00	–
	%**	0.45	0.26	0.71	53.29	53.29	5.54	5.54	19.31	8.26	5.28	0.93	0.41	0.19	0.12	34.50	1.75	1.75	1.86	0.19	1.15	0.26	3.46	0.60	0.15	0.75	100.00
Total Area	ha	10.00	1.90	11.90	697.41	697.41	1.16	1.16	584.65	400.75	2175.04	78.19	5.08	1.04	6.20	3250.95	40.20	40.20	524.99	3.78	50.03	4.05	582.85	44.93	10.39	55.32	**4639.79**
	%*	84.03	15.97	100.00	100.00	100.00	100.00	100.00	17.98	12.33	66.90	2.41	0.16	0.03	0.19	100.00	100.00	100.00	90.07	0.65	8.58	0.69	100.00	81.22	18.78	100.00	–
	%**	0.22	0.04	0.26	15.03	15.03	0.03	0.03	12.60	8.64	46.87	1.69	0.11	0.02	0.13	70.06	0.87	0.87	11.31	0.08	1.08	0.09	12.56	0.97	0.22	1.19	100.00
Active	ha	10.00	1.90	11.90	697.41	697.41	1.16	1.16	303.10	245.71	1187.31	0.00	5.08	1.04	0.00	1742.24	40.20	40.20	2.64	1.94	36.75	4.05	45.38	0.00	10.39	10.39	**2548.68**
	%*	84.03	15.97	100.00	100.00	100.00	100.00	100.00	9.32	7.56	36.52	0.00	0.16	0.03	0.00	53.59	100.00	100.00	0.45	0.33	6.31	0.69	7.79	0.00	18.78	18.78	–
	%**	0.39	0.07	0.46	27.36	27.36	0.05	0.05	11.89	9.64	46.60	0.00	0.20	0.04	0.00	68.37	1.57	1.57	0.10	0.08	1.44	0.16	1.78	0.00	0.41	0.41	100.00
Dormant	ha	–	–	–	–	–	–	–	281.58	155.08	987.65	78.20	0.00	0.00	0.00	1502.51	–	–	–	–	–	–	–	–	–	–	**1502.51**
	%*	–	–	–	–	–	–	–	8.66	4.77	30.38	2.41	0.00	0.00	0.00	46.22	–	–	–	–	–	–	–	–	–	–	–
	%**	–	–	–	–	–	–	–	18.74	10.32	65.74	5.20	0.00	0.00	0.00	100.00	–	–	–	–	–	–	–	–	–	–	100.00
Relict	ha	0.00	0.00	0.00	0.00	0.00	0.00	0.00	0.00	0.00	0.00	0.00	0.00	0.00	6.20	6.20	0.00	0.00	522.35	1.84	13.28	0.00	537.47	44.93	0.00	44.93	**588.60**
	%*	0.00	0.00	0.00	0.00	0.00	0.00	0.00	0.00	0.00	0.00	0.00	0.00	0.00	0.19	0.19	0.00	0.00	89.62	0.32	2.27	0.00	92.21	81.22	0.00	81.22	–
	%**	0.00	0.00	0.00	0.00	0.00	0.00	0.00	0.00	0.00	0.00	0.00	0.00	0.00	1.05	1.05	0.00	0.00	88.74	0.31	2.26	0.00	91.31	7.64	0.00	7.64	100.00
In evolution	ha	0.46	0.05	0.51	256.10	256.10	0.89	0.89	8.93	12.34	3.69	0.00	4.23	1.04	0.00	30.23	3.80	3.80	0.00	1.62	3.39	0.67	5.68	0.00	9.45	9.45	**306.66**
	%*	3.87	0.42	4.29	36.72	36.72	76.72	76.72	0.27	0.38	0.11	0.00	0.13	0.04	0.00	0.93	9.45	9.45	0.00	0.28	0.58	0.12	0.98	0.00	17.08	17.08	–
	%**	0.15	0.02	0.17	83.51	83.51	0.29	0.29	2.91	4.02	1.20	0.00	1.38	0.34	0.00	9.85	1.23	1.23	0.00	0.53	1.12	0.22	1.87	0.00	3.08	3.08	100.00
Stable	ha	8.36	0.36	8.72	182.85	182.85	0.15	0.15	499.07	271.23	1890.41	78.20	0.00	0.00	6.20	2745.11	30.08	30.08	522.35	0.67	29.38	3.37	555.77	26.79	0.00	26.79	**3549.47**
	%*	70.25	3.03	73.28	26.22	26.22	12.93	12.93	15.35	8.34	58.15	2.41	0.00	0.00	0.19	84.44	74.83	74.83	89.62	0.11	5.04	0.58	95.35	48.43	0.00	48.43	–
	%**	0.24	0.01	0.25	5.15	5.15	0.00	0.00	14.06	7.64	53.26	2.20	0.00	0.00	0.17	77.33	0.85	0.85	14.72	0.02	0.83	0.09	15.66	0.76	0.00	0.76	100.00
In regression	ha	1.17	1.50	2.67	258.46	258.46	0.12	0.12	76.73	117.21	280.81	0.00	0.86	0.00	0.00	475.61	6.32	6.32	2.64	1.50	17.26	0.00	21.40	18.14	0.94	19.08	**783.66**
	%*	9.83	12.60	22.43	37.06	37.06	10.35	10.35	2.36	3.60	8.64	0.00	0.03	0.00	0.00	14.63	15.72	15.72	0.45	0.26	2.96	0.00	3.67	32.79	1.70	34.49	–
	%**	0.15	0.19	0.34	32.98	32.98	0.03	0.03	9.79	14.96	35.83	0.00	0.11	0.00	0.00	60.69	0.80	0.80	0.34	0.19	2.20	0.00	2.73	2.31	0.12	2.43	100.00

Appendix B

The main results are made available for visualization in a dedicated WebGIS application that shows the components used for the elaboration of the HOTSED model and the related outputs. In particular, the *Potential of Sediment Sources* (PSS), *Structural Sediment Connectivity* (STC), *Potential for Sediment Transport* (PST), *Hotspot areas of Sediment Sources and delivery* (HSS) and the *Hazard Map of sediment Production and Delivery* (HPD) were reported together with the hillshade map and the Technical Regional Map at 1:5000 scale (Regione Emilia-Romagna, 2020a). The WebGIS implementation was developed through the ArcGIS online Web mapping Application (https://arcg.is/0Lf1zL) by Esri©. The advantage in using WebGIS platforms is a more effective accessibility of data to non-GIS specialists as well as their visualization with a proper detail (Maerker et al., 2019; Sartirana et al., 2020). Further improvements could be directed to the implementation of an online GIS decision-support system.

Appendix C

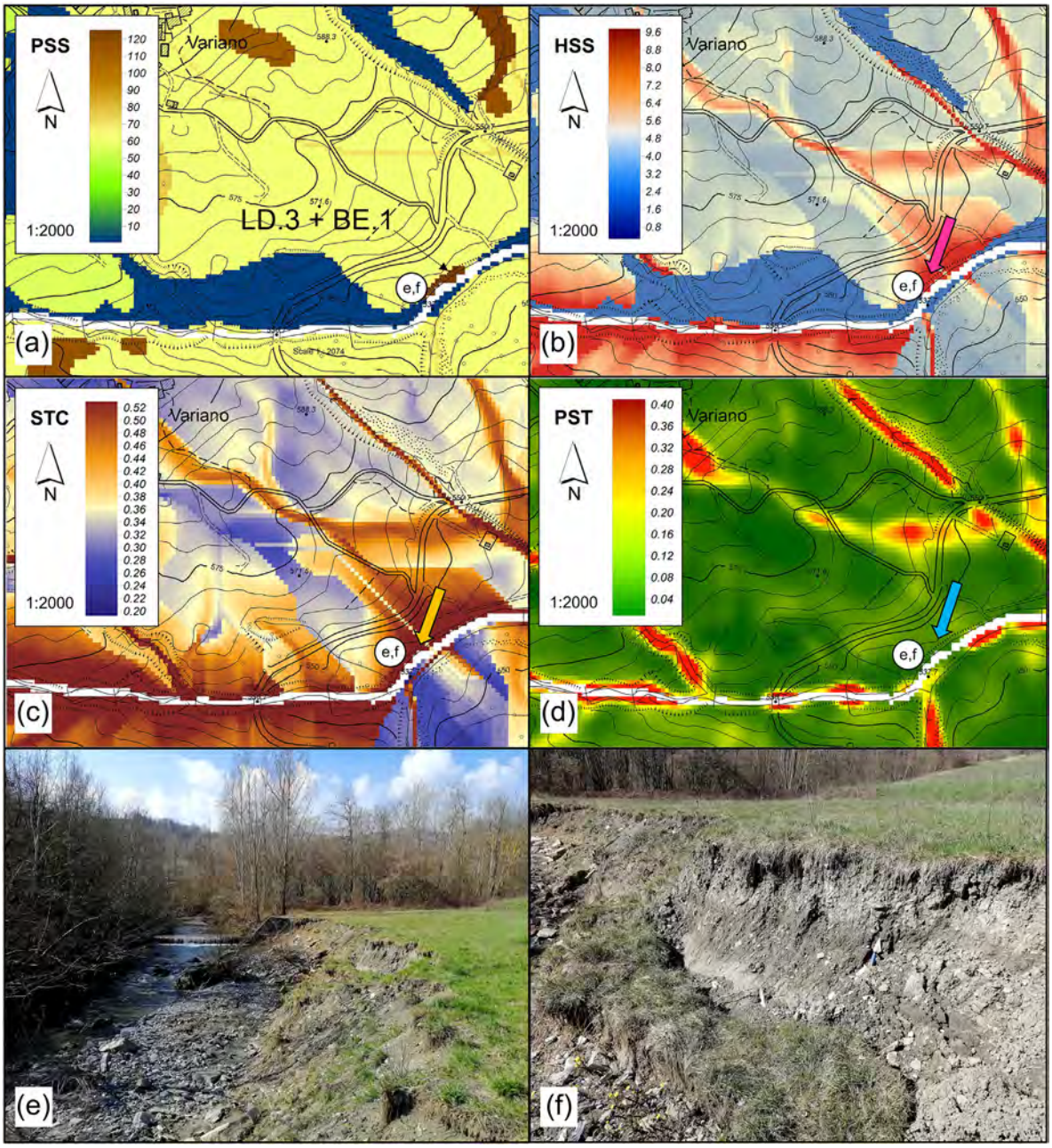

Fig. C.1. (a) The *Potential of Sediment Sources* (PSS) output map. The very high PSS value indicated by the arrow resulted from the summation of the total scores (Tot_scores) of the overlaying LD.3 and BE.1 geomorphic entities (*i.e.*, bank erosion at the landslide toe) (Fig. 4 and Fig. 5). (b) The *Hotspot areas of Sediment Sources and delivery* (HSS) output map shows very high values in correspondence of the bank erosion process (purple arrow). The proximity to the main channel (*i.e.*, Lubiana creek; Fig. 1) influences the (c) *Structural Sediment Connectivity* (STC), resulting in very high values (orange arrow). Conversely, the (d) *Potential for Sediment Transport* exhibits low values mainly due to the presence of gentle open slopes over the landslide toe (blue arrow). (e) Bank erosion at the toe of a large landslide body, which is continuously pouring out large amounts of sediment into the Lubiana creek (Fig. 1). (f) Chaotic material of gravitational-colluvial origin within the pedo-stratigraphic sequence of the riverbank. Pictures taken on 19/03/2024.

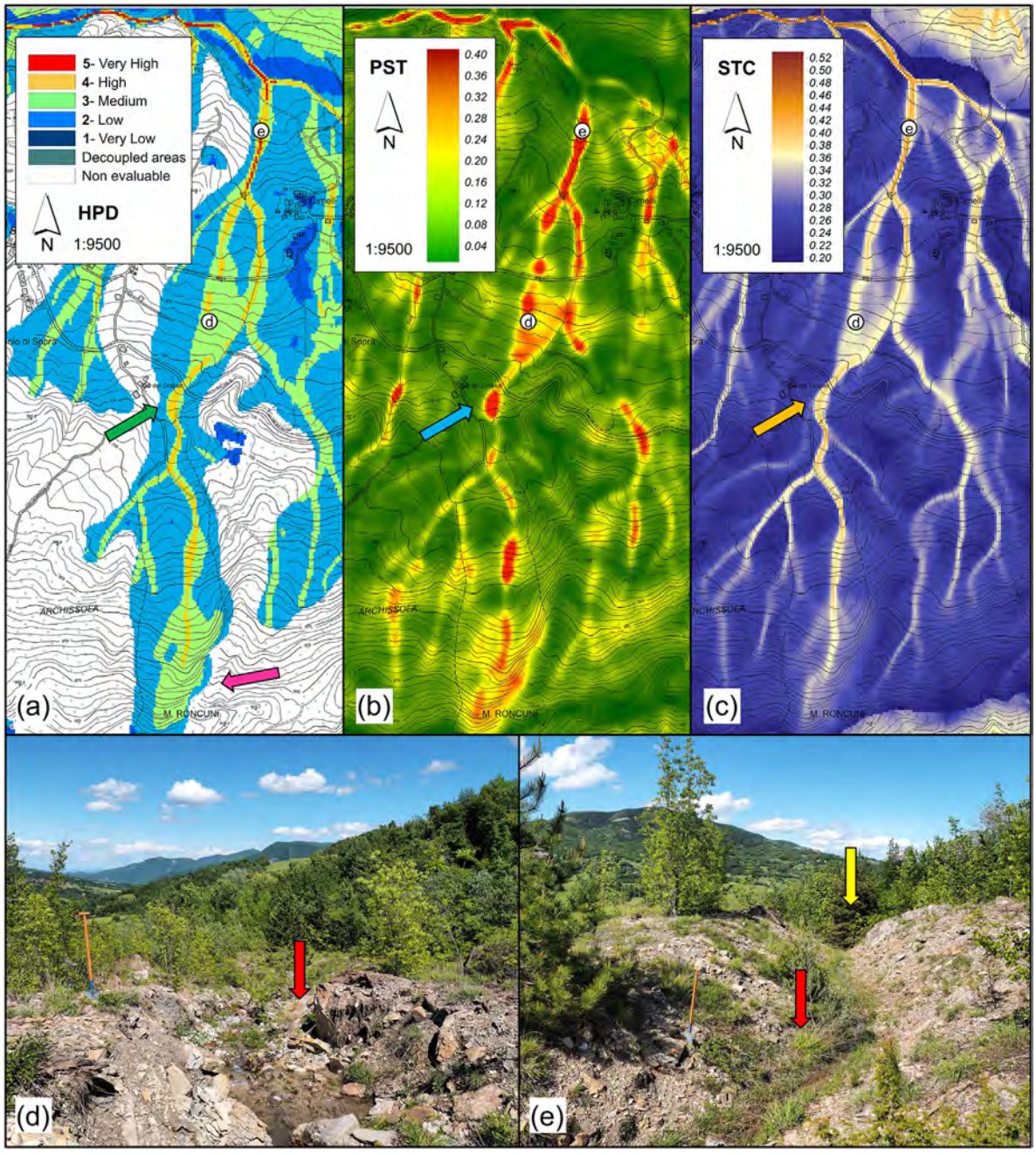

Fig. C.2. (a) *Hazard Map of sediment Production and Delivery* (HPD) (Fig. 10). A large landslide is characterized by a low relative hazard, with increasing hazard at the landslide main scarp (purple arrow). Moreover, hazard increases to medium, high, or very high along the drainages intersecting the landslide body (green arrow), as a function of increasing (b) *Potential for Sediment Transport* (PST) (blue arrow) and (c) *Structural Sediment Connectivity* (STC) (orange arrow). (d, e) Flowing water within the drainage which intersects the landslide body (red arrows). The main drainage of the landslide flows into another drainage with high to very high hazard (yellow arrow) before flowing into the Lubiana creek (Fig. 1). Pictures taken on 17/05/2024.

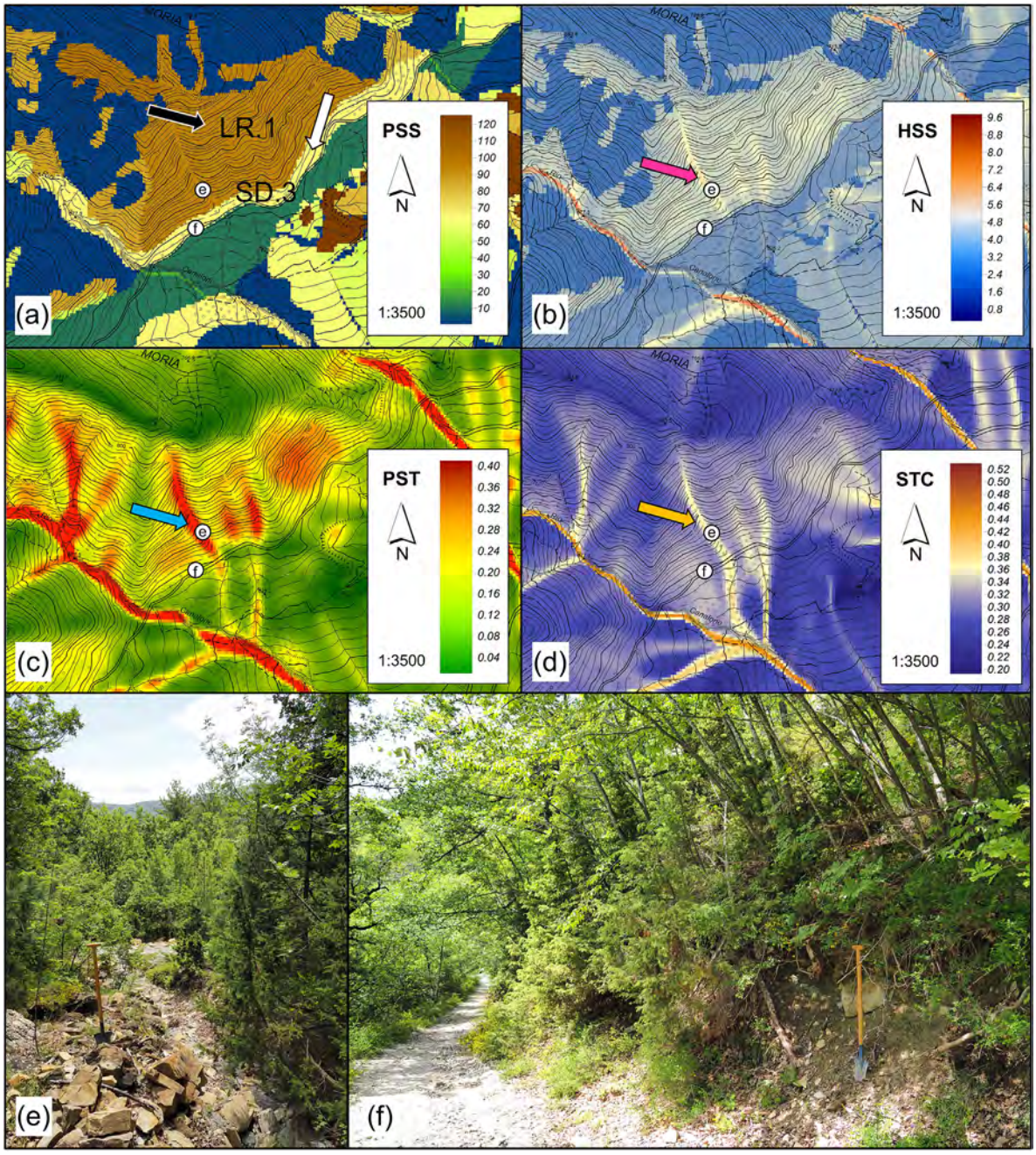

Fig. C.3. (a) The *Potential of Sediment Sources* (PSS) output map. The LR.1 geomorphic entity (black arrow; Fig. 5) has a homogeneous high geomorphic potential as it is an active, stable litho-structural-erosional system, characterized by rock/debris falls (*i.e.*, 'dominant processes'), debris flows (*i.e.*, 'secondary processes') and diffuse water runoff (*i.e.*, 'subordinate processes'). The SD.3 geomorphic entity (white arrow; Fig. 5) has a medium geomorphic potential as it is an active, stable talus deposited at the scarp base, characterized by continuous deposition of sediments from upslope areas (*i.e.*, 'dominant process') and affected by localized water runoff and small-scale debris flows (*i.e.*, 'subordinate processes). (b) The *Hotspot areas of Sediment Sources and delivery* (HSS) output map shows, on average, medium values for LR.1 and slightly decreased values for SD.3. Values are increasing along the midslope drainages which characterized the ribbon-line morphology (highlighted by the contour lines) (purple arrow), due to increasing values of (c) *Potential for Sediment Transport* (PST) (blue arrow) and (d) *Structural Sediment Connectivity* (STC) (orange arrow). (e) A couloir drainage filled with debris discharge, derived after debris flow occurrence, capable of reactivation during intense rainfall events. (f) Vegetated talus. The trail path marks the topographic discontinuity between upslope and downslope areas. Pictures taken on 17/05/2024.

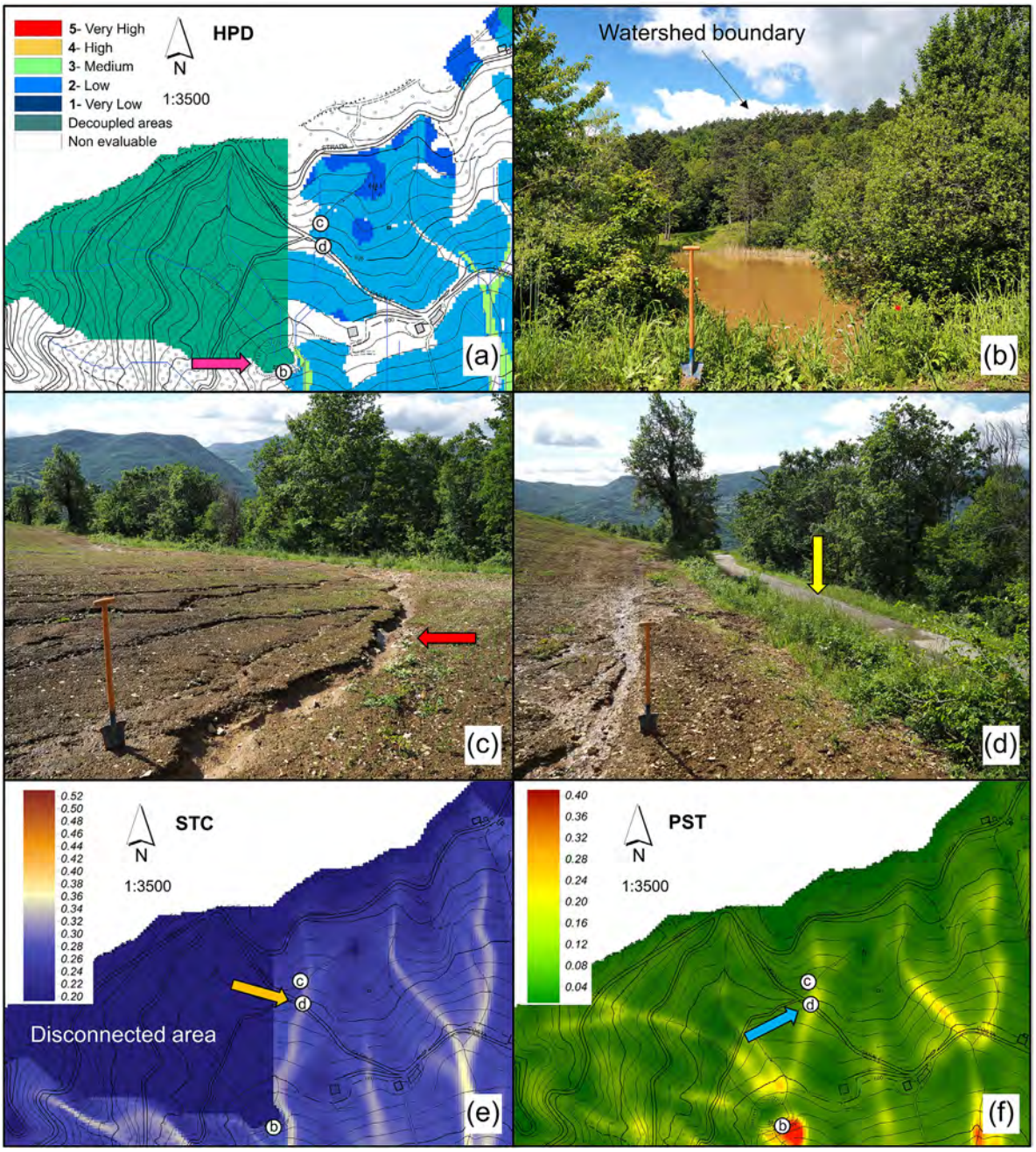

Fig. C.4. (a) *Hazard Map of sediment Production and Delivery* (HPD) (Fig. 10). (b) A natural pond is disconnecting the upstream area (purple arrow), which is classified as "decoupled area" in the HPD map. The picture shows the brownish colour of the water, emphasizing the high concentration of sediments trapped by the pond. (c, d) Evidence of active rill-interrill erosion on arable land. The red arrow indicates flowing water inside the rill. The yellow arrow indicates a flow path along the road, which moves water and sediments from upslope to downslope area. The geomorphic system shown in figures *c* and *d* is characterized, on average, by a low relative hazard, due to a combination of low-medium geomorphic potential (*i.e.*, PSS = 50), low (e) *Structural Sediment Connectivity* (STC), and low (f) *Potential for Sediment Transport* (PST). STC and PST values slightly increase along the drainage intersecting the road (orange and blue arrows, respectively). Pictures taken on 17/05/2024.

References

Abebe, N., Eekhout, J., Vermeulen, B., Boix-Fayos, C., de Vente, J., Grum, B., Hoitink, T., & Baartman, J. (2023). The potential and challenges of the 'RUSLE-IC-SDR' approach to identify sediment dynamics in a Mediterranean catchment. *Catena, 233*, Article 107480. https://doi.org/10.1016/j.catena.2023.107480

Alewell, C., Borrelli, P., Meusburger, K., & Panagos, P. (2019). International Soil and Water Conservation Research. *Int. Soil Water Conserv. Res., 7*(3), 203–225. https://doi.org/10.1016/j.iswcr.2019.05.004

Angileri, A. E., Conoscenti, C., Hochschild, V., Maerker, M., Rotigliano, E., & Agnesi, V. (2016). Water erosion susceptibility mapping by applying Stochastic gradient treeboost to the imera meridionale river basin (sicily, Italy). *Geomorphology, 262*, 61–76. https://doi.org/10.1016/j.geomorph.2016.03.018

APAT - Agenzia per la Protezione dell'Ambiente e per i Servizi Tecnici. (2007). *Rapporto sulle frane in Italia. Il Progetto IFFI – Metodologia, risultati e rapporti regionali*. Rapporti APAT 78/2007, Roma.

Bartsch, A., Gude, M., Jonasson, C., & Scherer, D. (2002). Identification of geomorphic process units in Kiirkevagge, northern Sweden, by remote sensing and digital terrain analysis. *Geografiska Annaler, 84 A*(3–4), 171–178.

Battaglia, S., Leoni, L., & Sartori, F. (2002). Mineralogical and grain size composition of clays developing Calanchi and biancane erosional landforms. *Geomorphology, 49*(1–2), 153–170. https://doi.org/10.1016/S0169-555X(02)00171-X

Bertolini, G., Casagli, N., Ermini, L., & Malaguti, C. (2004). Radiocarbon data on lateglacial and holocene landslides in the northern Apennines. *Natural Hazards,*

31(3), 645–662. https://doi.org/10.1023/B:NHAZ.0000024896.34933.63

Bertolini, G., Corsini, A., & Tellini, C. (2017). Fingerprints of large-scale landslides in the landscape of the Emilia Apennines. In M. Soldati, & M. Marchetti (Eds.), *Landscapes and landforms of Italy. World geomorphological landscape* (pp. 215–224). Springer International Publishing AG. https://doi.org/10.1007/978-3-319-26194-2_18.

Bertolini, G., Guida, M., & Pizziolo, M. (2005). Landslides in emilia-romagna region (Italy): Strategies for hazard assessment and risk management. *Landslides, 2*(4), 302–312. https://doi.org/10.1007/s10346-005-0020-1

Bertolini, G., & Pizziolo, M. (2004). Landslides of the Emilia Apennines (northern Italy). *32nd International Geological Congress, 3*. from D01 to P13, Florence, Italy.

Bertolini, G., & Pizziolo, M. (2008). Risk assessment strategies for the reactivation of earth flows in the Northern Apennines (Italy). *Engineering Geology, 102*(3–4), 178–192. https://doi.org/10.1016/j.enggeo.2008.03.017

Bertolini, G., & Tellini, C. (2001). New radiocarbon dating for landslide occurrences in the Emilia Apennines (Northern Italy). *Trans Japan. Geom. Un., 22*(4), C-23.

Bishop, M. P., James, L. A., Shroder, J. F., & Walsh, S. J. (2012). Geospatial technologies and digital geomorphological mapping: Concepts, issues and research. *Geomorphology, 137*, 5–26. https://doi.org/10.1016/j.geomorph.2011.06.027

Borgatti, L., Corsini, A., Barbieri, M., Sartini, G., Truffelli, G., Caputo, G., & Puglisi, C. (2006). Large reactivated landslides in weak rock masses: A case study from the northern Apennines (Italy). *Landslides, 3*(2), 115–124. https://doi.org/10.1007/s10346-005-0033-9

Borrelli, P., Maerker, M., Panagos, P., & Schütt, B. (2014). Modelling soil erosion and river sediment yield for an intermountain drainage basin of the Central Apennines, Italy. *Catena, 114*, 45–58. https://doi.org/10.1016/j.catena.2013.10.007

Borrelli, P., Oost, K., Meusburger, K., Alewell, C., Lugato, E., & Panagos, P. (2018). A step towards a holistic assessment of soil degradation in europe: Coupling on-site erosion with sediment transfer and carbon fluxes. *Environmental Research, 161*, 291–298. https://doi.org/10.1016/j.envres.2017.11.009

Borselli, L., Cassi, P., & Torri, D. (2008). Prolegomena to sediment and flow connectivity in the landscape: A GIS and field numerical assessment. *Catena, 75*, 268–277. https://doi.org/10.1016/j.catena.2008.07.006

Bosino, A., Omran, A., & Maerker, M. (2019). Identification and analysis of the oltrepo pavese calanchi in the northern Apennines (Italy). *Geomorphology, 340*, 53–66. https://doi.org/10.1016/j.geomorph.2019.05.003

Bosino, A., Szatten, D. A., Omran, A., Crema, S., Crozi, M., Becker, R., Bettoni, M., Schillaci, C., & Maerker, M. (2022). Assessment of suspended sediment dynamics in a small ungauged badland catchment in the Northern Apennines (Italy) using an in-situ laser diffraction method. *Catena, 209*, Article 105796. https://doi.org/10.1016/j.catena.2021.105796

Bracken, L. J., Turnbull, L., Wainwright, J., & Bogaart, P. (2015). Sediment connectivity: A framework for understanding sediment transfer at multiple scales. *Earth Surface Processes and Landforms, 40*, 177–188. https://doi.org/10.1002/esp.3635

Bracken, L. J., Wainwright, J., Ali, G. A., Tetzlaff, D., Smith, M. W., Reaney, S. M., & Roy, A. G. (2013). Concepts of hydrological connectivity: Research approaches, pathways and future agendas. *Earth-Science Reviews, 119*, 17–34. https://doi.org/10.1016/j.earscirev.2013.02.001

Brardinoni, F., Cavalli, M., Heckmann, T., Liebault, F., & Rimbock, A. (2015). Guidelines for assessing sediment dynamics in Alpine basins and channel reaches. *Final project report (WP4)*. Alpine Space Programme – SedAlp Project.

Brierley, G., Fryirs, K., & Jain, V. (2006). Landscape connectivity: The geographical basis of geomorphic applications. *Area, 38*(2), 165–174. https://doi.org/10.1111/j.1475-4762.2006.00671.x

Buter, A., Heckmann, T., Filisetti, L., Savi, S., Mao, L., Gems, B., & Comiti, F. (2022). Effects of catchment characteristics and hydro-meteorological scenarios on sediment connectivity in glacierised catchments. *Geomorphology, 402*, Article 108128. https://doi.org/10.1016/j.geomorph.2022.108128

Camerano, P, Varese, P., & Grieco, C (2006). *Classificazione di popolamenti forestali dell'Emilia-Romagna di supporto alla pianificazione forestal*. Regione Emilia-Romagna: IPLA S.p.A. Direzione Generale all'Ambiente e Difesa del Suolo e della Costa, Regione Emilia-Romagna.

Campobasso, C., Carton, A., Chelli, A., D' Orefice, M., Dramis, F., Graciotti, R., … Pellegrini, L. (2021). *Aggiornamento ed integrazioni delle linee guida della Carta Geomorfologica d'Italia alla scala 1:50000 e banca dati geomorfologica. Carta Geomorfologica d'Italia alla scala 1:50000. Fascicolo I, Versione 2.0*. Roma: Istituto Poligrafico e Zecca dello Stato. Quaderni del Servizio Geologico Nazionale, Ser. III, 13.

Carlini, M., Chelli, A., Vescovi, P., Artoni, A., Clemenzi, L., Tellini, C., & Torelli, L. (2016). Tectonic control on the development and distribution of large landslides in the Northern Apennines. *Geomorphology, 253*, 425–437. https://doi.org/10.1016/j.geomorph.2015.10.028

Castaldi, F., & Chiocchini, U. (2012). Effects of land use changes on badland erosion in clayey drainage basins, Radiocofani, Central Italy. *Geomorphology, 169–170*, 98–108. https://doi.org/10.1016/j.geomorph.2012.04.016

Cavalli, M., Crema, S., & Marchi, L. (2014). Guidelines on the sediment connectivity stand-alone application SedInConnect. Release: 2.0 (and 2.1). Sediment management in alpine basins – SedAlp project. www.sedalp.eu.

Cavalli, M., Trevisani, S., Comiti, F., & Marchi, L. (2013). Geomorphometric assessment of spatial sediment connectivity in small Alpine catchments. *Geomorphology, 188*, 31–41. https://doi.org/10.1016/j.geomorph.2012.05.007

Cendrero, A., Forte, L. M., Remondo, J., & Cuesta-Albertos, J. A. (2020). Anthropocene geomorphic change. Climate or human activities? *Earth's Future, 8*, Article e2019EF001305. https://doi.org/10.1029/2019EF001305

Cerdà, A., Rodrigo-Comino, J., Novara, A., Brevik, E. C., Vaezi, A. R., Pulido, M., Giménez-Morera, A., & Keesstra, S. D. (2018). Long-term impact of rainfed agricultural land abandonment on soil erosion in the Western Mediterranean basin. *Progress in Physical Geography, 42*(2), 202–219. https://doi.org/10.1177/0309133318758521

Chen, C., Tfwala, S. S., & Tsai, C. (2020). Climate change impacts on soil erosion and sediment yield in a watershed. *Water, 12*(8), 2247. https://doi.org/10.3390/w12082247

Cho, S. J., Karwan, D. L., Skalak, K., Pizzuto, J., & Human, M. E. (2023). Sediment sources and connectivity linked to hydrologic pathways and geomorphic processes: A conceptual model to specify sediment sources and pathways through space and time. *Front Water, 5*, Article 1241622. https://doi.org/10.3389/frwa.2023.1241622

Cislaghi, A., & Bischetti, G. B. (2019). Source areas, connectivity, and delivery rate of sediments in mountainous-forested hillslopes: A probabilistic approach. *The Science of the Total Environment, 652*, 1168–1186. https://doi.org/10.1016/j.scitotenv.2018.10.318

Conrad, O., Bechtel, B., Bock, M., Dietrich, H., Fischer, E., Gerlitz, L., Wehberg, J., Wichmann, V., & Böhner, J. (2015). System for automated geoscientific analyses (SAGA) v. 2.1.4. *Geoscientific Model Development, 8*(7), 1991–2007. https://doi.org/10.5194/gmd-8-1991-2015

Conti, P., Cornamusini, G., & Carmignani, L. (2020). An outline of the geology of the Northern Apennines (Italy), with geological map at 1:250000 scale. *Italian Journal of Geosciences, 139*(2), 149–194. https://doi.org/10.3301/IJG.2019.25

Coratza, P., & Parenti, C. (2021). Controlling factors on badland morphological changes in the Emilia Apennines (northern Italy). *Water, 13*(4), 539. https://doi.org/10.3390/w13040539

Costantini, E. A. C., & Lorenzetti, R. (2013). Soil degradation processes in the Italian agricultural and forest ecosystems. *Italian Journal of Agronomy, 8*(4), 233–243. https://doi.org/10.4081/ija.2013.e28

Crema, S., & Cavalli, M. (2018). SedInConnect: A stand-alone, free and open source tool for the assessment of sediment connectivity. *Computers & Geosciences, 111*, 39–45. https://doi.org/10.1016/j.cageo.2017.10.009

Crema, S., Schenato, L., Goldin, B., Marchi, L., & Cavalli, M. (2015). Toward the development of a stand-alone application for the assessment of sediment connectivity. *Rendiconti della Societa Geologica Italiana, 34*, 58–61. https://doi.org/10.3301/ROL.2015.37

Cruden, D. M., & Varnes, D. J. (1996). Landslide types and processes. In A. K. Turner, & R. L. Schuster (Eds.), *Landslide investigation and mitigation* (pp. 36–75). Transportation research board, US National Research Council. Special Report 247, Washington DC, Chapter 3.

de Vente, J., Poesen, J., Bazzoffi, P., Van Rompaey, A., & Verstraeten, G. (2006). Predicting catchment sediment yield in mediterranean environments: The importance of sediment sources and connectivity in Italian drainage basins. *Earth Surface Processes and Landforms, 31*(8), 1017–1034. https://doi.org/10.1002/esp.1305

Dumitriu, D., Rădoane, M., & Rădoane, N. (2017). Sediment sources and delivery. In M. Rădoane, & A. Vespremeanu-Stroe (Eds.), *Landform dynamics and evolution in Romania* (pp. 629–654). Springer Geography, Springer Cham.. https://doi.org/10.1007/978-3-319-32589-7_27

Fabre, C., Fressard, M., Bizzi, S., Branger, F., & Piegay, H. (2024). Combining hillslope erosion and river connectivity models to assess large scale fine sediment transfers: Application over the Rhône River (France). *Earth Surface Processes and Landforms*, 1–19. https://doi.org/10.1002/esp.5874

FAO. (2019). *Soil erosion: The greatest challenge to sustainable soil management*. Rome.

Ferreira, C. S. S., Seifollahi-Aghmiuni, S., Destouni, G., Ghajarnia, N., & Kalantari, Z. (2022). Soil degradation in the European Mediterranean region: Processes, status and consequences. *The Science of the Total Environment, 805*, Article 150106. https://doi.org/10.1016/j.scitotenv.2021.150106

Fryirs, K. (2013). (Dis)Connectivity in catchment sediment cascades: A fresh look at sediment delivery problem. *Earth Surface Processes and Landforms, 38*, 30–46. https://doi.org/10.1002/esp.324

Fryirs, K. A., Brierley, G. J., Preston, N. J., & Kasai, M. (2007). Buffers, barriers and blankets: The (dis)connectivity of catchment-scale sediment cascades. *Catena, 70*, 49–67. https://doi.org/10.1016/j.catena.2006.07.007

García-Orenes, F., Morugán-Coronado, A., Zornoza, R., Cerdà, A., & Scow, K. (2013). Changes in soil microbial community structure influenced by agricultural management practices in a mediterranean agro-ecosystem. *PLoS One, 8*(11), Article e80522. https://doi.org/10.1371/journal.pone.0080522

García-Orenes, F., Roldán, A., Mataix-Solera, J., Cerdà, A., Campoy, M., Arcenegui, V., & Caravaca, F. (2012). Soil structural stability and erosion rates influenced by agricultural management practices in a semi-arid Mediterranean agro-ecosystem. *Soil Use & Management, 28*(4), 571–579. https://doi.org/10.1111/j.1475-2743.2012.00451.x

Gellis, A., Fitzpatrick, F., & Schubauer-Berigan, J. (2016). *A manual to identify sources of fluvial sediment. Office of research and development, national risk management research laboratory, land remediation and pollution control division*. United States Environmental Protection Agency. EPA/600/R-16/210.

Gellis, A. C., & Walling, D. E. (2011). Sediment-source fingerprinting (tracing) and sediment budgets as tools in targeting river and watershed restoration programs. In A. Simon, S. Bennett, & J. M. Castro (Eds.), *Stream restoration in dynamic fluvial systems: Scientific approaches, analyses, and tools* (Vol 194, pp. 263–291). American Geophysical Union Monograph Series.

Goldin, B. (2015). *Geomorphometric analysis and sediment dynamics in mountainous basins: Spatial and temporal scales*. Università degli Studi di Padova. Doctoral Thesis.

Gozza, G., & Pizziolo, M. (2007). Analisi del dissesto da frana in Emilia-Romagna. Agenzia per la Protezione dell'Ambiente e per i Servizi Tecnici. In *Rapporto sulle frane in Italia. Il Progetto IFFI – Metodologia, risultati e rapporti regionali* (pp. 329–353). Rapporti APAT 78/2007, Roma.

Grauso, S., Pasanisi, F., & Tebano, C. (2018). Assessment of a simplified connectivity index and specific sediment potential in river basins by means of geomorphometric tools. *Geosciences, 8*(2), 48. https://doi.org/10.3390/geosciences8020048

Gude, M., Daut, G., Dietrich, S., Mäusbacher, R., Jonasson, C., Bartsch, A., & Scherer, D. (2002). Towards an integration of process measurements, archive analysis and modelling in geomorphology – the Kärkevagge experimental site, Abisko area, northern Sweden. *Geografiska Annaler, 84A*(3–4), 205–212.

Guo, Z., Wu, L., Shuai, L., Zhang, H., Du, B., & Ruan, B. (2023). An integrated watershed modelling framework to explore the covariation between sediment connectivity and soil erosion. *European Journal of Soil Science, 74*, Article e13412. https://doi.org/10.1111/ejss.13412

Hamel, P., Falinski, K., Sharp, R., Auerbach, D. A., Sanchez-Canales, M., & Dennedy-Frank, P. J. (2017). Sediment delivery modeling in practice: Comparing the effects of watershed characteristics and data resolution across hydroclimatic regions. *The Science of the Total Environment, 580*, 1381–1388. https://doi.org/10.1016/j.scitotenv.2016.12.103

Hao, R., Huang, X., Cai, Z. W., Xiao, H. B., Wang, J., & Shi, Z. H. (2022). Incorporating sediment connectivity index into MUSLE model to explore soil erosion and sediment yield relationships at event scale. *Journal of Hydrology, 614*, Article 128579. https://doi.org/10.1016/j.jhydrol.2022.128579

Harvey, A. M. (2002). Effective timescales of coupling within fluvial systems. *Geomorphology, 44*(3–4), 175–201. https://doi.org/10.1016/S0169-555X(01)00174-X

Heckmann, T., Cavalli, M., Cerdan, O., Foerster, S., Javaux, M., Lode, E., & Brardinoni, F. (2018). Indices of sediment connectivity: Opportunities, challenges and limitations. *Earth-Science Reviews, 187*, 77–108. https://doi.org/10.1016/j.earscirev.2018.08.004

Heckmann, T., & Schwanghart, W. (2013). Geomorphic coupling and sediment connectivity in an alpine catchment — exploring sediment cascades using graph theory. *Geomorphology, 182*, 89–103. https://doi.org/10.1016/j.geomorph.2012.10.033

Hoffmann, T. (2015). Sediment residence time and connectivity in non-equilibrium and transient geomorphic systems. *Earth-Science Reviews, 150*, 609–627. https://doi.org/10.1016/j.earscirev.2015.07.008

Hooke, J., & Souza, J. (2021). Challenges of mapping, modelling and quantifying sediment connectivity. *Earth-Science Reviews, 223*, Article 103847. https://doi.org/10.1016/j.earscirev.2021.103847

Hooke, J., Souza, J., & Marchamalo, M. (2021). Evaluation of connectivity indices applied to a Mediterranean agricultural catchment. *Catena, 207*, Article 105713. https://doi.org/10.1016/j.catena.2021.105713

Hungr, O., Leroueil, S., & Picarelli, L. (2014). The Varnes classification of landslide types, an update. *Landslides, 11*, 167–194. https://doi.org/10.1007/s10346-013-0436-y

IAEG – International Association Engineering Geology Commission on Landslides. (1990). Suggested nomenclature for landslides. *Bulletin of the International Association of Engineering Geology, 41*, 13–16.

IUGS/WGL – International Union of Geological Science Working Group on Landslides. (1995). A suggested method for describing the rate of movement of a landslide. *Bulletin of the International Association of Engineering Geology, 52*, 75–78.

IUSS Working Group WRB. (2015). *World Reference Base for Soil Resources 2014, update 2015. International soil classification system for naming soils and creating legends for soil maps. World Soil Resources Reports No. 106*. Rome: FAO.

Jenks, G. F. (1967). The data model concept in statistical mapping. *International Yearbook of Cartography, 7*, 186–190.

Kondolf, G. M., & Podolak, K. (2014). Space and time scales in human-landscape systems. *Environmental Manager, 53*, 76–87. https://doi.org/10.1007/s00267-013-0078-9

Kottek, M., Grieser, J., Beck, C., Rudolf, B., & Rubel, F. (2006). World Map of the Köppen-Geiger climate classification updated. *Meteorologische Zeitschrift, 15*(3), 259–263. https://doi.org/10.1127/0941-2948/2006/0130

La Licata, M., Bosino, A., Bettoni, M., & Maerker, M. (2023). Assessing landscape features and geomorphic processes influencing sediment dynamics in a geomorphologically highly active Mediterranean agroecosystem: The upper Val d'Arda case study (Northern Apennines, Italy). *Geomorphology, 433*, Article 108724. https://doi.org/10.1016/j.geomorph.2023.108724

Le Houérou, H. N. (1993). Land degradation in mediterranean europe: Can agroforestry be a part of the solution? A prospective review. *Agroforestry Systems, 21*, 43–61. https://doi.org/10.1007/bf00704925

Li, Z., & Fang, H. (2016). Impacts of climate change on water erosion: A review. *Earth-Science Reviews, 163*, 94–117. https://doi.org/10.1016/j.earscirev.2016.10.004

Lidberg, W., Nilsson, M., Lundmark, T., & Ågren, A. M. (2017). Evaluating preprocessing methods of digital elevation models for hydrological modelling. *Hydrological Processes, 31*(26), 4623–4761. https://doi.org/10.1002/hyp.11385

Liu, Y., & Fu, B. (2016). Assessing sedimentological connectivity using WATEM/SEDEM model in a hilly and gully watershed of the Loess Plateau, China. *Ecological Indicators, 66*, 259–268. https://doi.org/10.1016/j.ecolind.2016.01.055

Lizaga, I., Gaspar, L., Latorre, B., & Navas, A. (2020). Variations in transport of suspended sediment and associated elements induced by rainfall and agricultural cycle in a Mediterranean agroforestry catchment. *Journal of Environmental Management, 272*, Article 111020. https://doi.org/10.1016/j.jenvman.2020.111020

Lizaga, I., Quijano, L., Gaspar, L., Ramos, M. C., & Navas, A. (2019). Linking land use changes to variation in soil properties in a Mediterranean mountain agroecosystem. *Catena, 172*, 516–527. https://doi.org/10.1016/j.catena.2018.09.019

Lizaga, I., Quijano, L., Palazón, L., Gaspar, L., & Navas, A. (2018). Enhancing Connectivity Index to assess the effects of land use changes in a Mediterranean catchment. *Land Degradation & Development, 29*(3), 663–675. https://doi.org/10.1002/ldr.2676

Llena, M., Vericat, D., Cavalli, M., Crema, S., & Smith, M. W. (2019). The effects of land use and topographic changes on sediment connectivity in mountain catchments. *The Science of the Total Environment, 660*, 899–912. https://doi.org/10.1016/j.scitotenv.2018.12.479

López-Vicente, M., & Ben-Salem, N. (2019). Computing structural and functional flow and sediment connectivity with a new aggregated index: A case study in a large mediterranean catchment. *The Science of the Total Environment, 651*, 179–191. https://doi.org/10.1016/j.scitotenv.2018.09.170

López-Vicente, M., & Navas, A. (2010). Relating soil erosion and sediment yield to geomorphic features and erosion processes at the catchment scale in the Spanish Pre-Pyrenees. *Environmental Earth Sciences, 61*, 143–158. https://doi.org/10.1007/s12665-009-0332-x

Maerker, M., Bosino, A., Scopesi, C., Giordani, P., Firpo, M., & Rellini, I. (2020). Assessment of calanchi and rill-interril erosion susceptibility in northern liguria, Italy: A case study using a probabilistic modelling framework. *Geoderma, 371*, Article 114367. https://doi.org/10.1016/j.geoderma.2020.114367

Maerker, M., Moretti, S., & Rodolfi, G. (2001). Assessment of water erosion processes and dynamics in semi-arid regions of southern Africa (KwaZulu/Natal RSA, and Swaziland) using the Erosion Response Units Concept (ERU). *Geografia Fisica e Dinamica Quaternaria, 24*, 71–83.

Maerker, M., Schillaci, C., & Kropáček, J. (2018). Morphometric terrain analysis to explore present day geohazards and paleolandscape forms and features in the surroundings of the Melka Kunture prehistoric site, Upper Awash Valley, Central Ethiopia. *AUC Geographica, 53*(1), 10–19. https://doi.org/10.14712/23361980.2018.2

Maerker, M., Schillaci, C., Melis, R. T., Kropáček, J., Bosino, A., Vilímek, V., Hochschild, V., Sommer, C., Altamura, F., & Mussi, M. (2019). Geomorphological processes, forms and features in the surroundings of the Melka Kunture Palaeolithic site, Ethiopia. *Journal of Maps, 15*(2), 797–806. https://doi.org/10.1080/17445647.2019.1669497

Mahoney, D., Blandford, B., & Fox, J. (2021). Coupling the probability of connectivity and RUSLE reveals pathways of sediment transport and soil loss rates for forest and reclaimed mine landscape. *Journal of Hydrology, 594*, Article 125963. https://doi.org/10.1016/j.jhydrol.2021.125963

Marroni, M., Molli, G., Ottria, G., & Pandolfi, L. (2001). Tectono-sedimentary evolution of the external liguride units (northern Apennines, Italy): Insights in the pre-collisional history of a fossil ocean-continent transition zone. Geodin. *Acta, 14*(5), 307–320. https://doi.org/10.1016/S0985-3111(00)01050-0

Martini, A., & Zanzucchi, G. (2000). *Note Illustrative della Carta Geologica d'Italia alla scala 1:50000, Foglio 198 - Bardi* (p. 102). Roma: Servizio Geologico d'Italia.

Martín-López, B., Oteros-Rozas, E., Cohen-Shacham, E., Santos-Martín, F., Nieto-Romero, M., Carvalho-Santos, C., González, J. A., García-Llorente, M., Klass, K., Geijzendorffer, I., Montes, C., & Cramer, W. (2016). Ecosystem services supplied by mediterranean basin ecosystems. In M. Potschin, R. Haines-Young, R. Fish, & R. K. Turner (Eds.), *Handbook of ecosystem services* (1st ed., pp. 405–414). Routledge.

Martini, L., Cavalli, M., & Picco, L. (2022). Predicting sediment connectivity in a mountain basin: A quantitative analysis of the index of connectivity. *Earth Surface Processes and Landforms*, 1–14. https://doi.org/10.1002/esp.5331

Messenzehl, K., Hoffmann, T., & Dikau, R. (2014). Sediment connectivity in the high-alpine valley of Val Müschauns, Swiss National Park — linking geomorphic field mapping with geomorphometric modelling. *Geomorphology, 221*, 215–229. https://doi.org/10.1016/j.geomorph.2014.05.033

Michalek, A., Zarnaghsh, A., & Husic, A. (2021). Modeling linkages between erosion and connectivity in an urbanizing landscape. *The Science of the Total Environment, 764*, Article 144255. https://doi.org/10.1016/j.scitotenv.2020.144255

Montgomery, D. R. (2007). Soil erosion and agricultural sustainability. *Proceedings of the National Academy of Sciences, 4*(33), 13268–13272. https://doi.org/10.1073/pnas.0611508104

Moore, I. D., Grayson, R. B., & Ladson, A. R. (1991). Digital terrain modelling: A review of hydrological, geomorphological, and biological applications. *Hydrological Processes, 5*(1), 3–30. https://doi.org/10.1002/hyp.3360050103

Moore, I. D., & Nieber, J. L. (1989). Landscape assessment of soil erosion and nonpoint source pollution. J. Minnesota Acad. *Scientia, 55*, 18–25.

Najafi, S., Dragovich, D., Heckmann, T., & Sadeghi, S. H. (2021a). Sediment connectivity concepts and approaches. *Catena, 196*, Article 104880. https://doi.org/10.1016/j.catena.2020.104880

Najafi, S., Sadeghi, S. H., & Heckmann, T. (2021b). Analysis of sediment accessibility and availability concepts based on sediment connectivity throughout a watershed. *Land Degradation & Development, 32*(10), 3023–3044. https://doi.org/10.1002/ldr.3964

Nicoletti, P. G., & Sorriso-Valvo, M. (1991). Geomorphic controls of the shape and mobility of rock avalanches. *The Geological Society of America Bulletin, 103*(10),

1365–1373. https://doi.org/10.1130/0016-7606(1991)103%3C1365:GCOTSA%3E2.3.CO;2

Nieto-Romero, M., Oteros-Rozas, E., González, J. A., & Martín-López, B. (2014). Exploring the knowledge landscape of ecosystem services assessments in Mediterranean agroecosystems: Insights for future research. *Environmental Science & Policy, 37*, 121–133. https://doi.org/10.1016/j.envsci.2013.09.003

Olaya, V., & Conrad, O. (2009). Geomorphometry in SAGA. In T. Hengl, & H. Reuter (Eds.), *Geomorphometry. Concepts, software, applications. Developments in soil science* (Vol 33, pp. 293–308). Elsevier. https://doi.org/10.1016/S0166-2481(08)00012-3.

Olsson, L., Barbosa, H., Bhadwal, S., Cowie, A., Delusca, K., Flores-Renteria, D., Hermans, K., Jobbagy, E., Kurz, W., Li, D., Sonwa, D. J., & Stringer, L. (2019). Land degradation. In P. R. Shukla, J. Skea, E. Calvo Buendia, V. Masson-Delmotte, H.-O. Pörtner, D. C. Roberts, P. Zhai, R. Slade, S. Connors, R. van Diemen, M. Ferrat, E. Haughey, S. Luz, S. Neogi, M. Pathak, J. Petzold, J. Portugal Pereira, P. Vyas, E. Huntley, & J. Malley (Eds.), *Climate change and land: An IPCC special report on climate change, desertification, land degradation, sustainable land management, food security, and greenhouse gas fluxes in terrestrial ecosystems*. https://doi.org/10.1017/9781009157988.006

Panagos, P., Ballabio, C., Borrelli, P., Meusburger, K., Klik, A., Rousseva, S., Tadic, M. P., Michaelides, S., Hrabalíková, M., Olsen, P., Aalto, J., Lakatos, M., Rymszewicz, A., Dumitrescu, A., Begueria, S., & Alewell, C. (2015a). Rainfall erosivity in europe. *The Science of the Total Environment, 511*, 801–814. https://doi.org/10.1016/j.scitotenv.2015.01.008

Panagos, P., Borrelli, P., Meusburger, C., Alewell, C., Lugato, E., & Montanarella, L. (2015b). Estimating the soil erosion cover-management factor at European scale. *Land Use policy journal, 48C*, 38–50. https://doi.org/10.1016/j.landusepol.2015.05.021

Panagos, P., Borrelli, P., Poesen, J., Ballabio, C., Lugato, E., Meusburger, K., Montanarella, L., & Alewell, C. (2015c). The new assessment of soil loss by water erosion in Europe. *Environmental Science & Policy, 54*, 438–447. https://doi.org/10.1016/j.envsci.2015.08.0122015e

Panagos, P., Van Liedekerke, M., Borrelli, P., Köninger, J., Ballabio, C., Orgiazzi, A., Lugato, E., Liakos, L., Hervas, J., Jones, A., & Montanarella, L. (2022). European Soil Data Centre 2.0: Soil data and knowledge in support of the EU policies. *European Journal of Soil Science, 73*(6), Article e13315. https://doi.org/10.1111/ejss.13315

Patro, E. R., De Michele, C., Granata, G., & Biagini, C. (2022). Assessment of current reservoir sedimentation rate and storage capacity loss: An Italian overview. *Journal of Environmental Management, 320*, Article 115826. https://doi.org/10.1016/j.jenvman.2022.115826

Pellegrini, L., & Vercesi, P. L. (2017). Landscape and landforms driven by geological structures in the northwestern Apennines. In M. Soldati, & M. Marchetti (Eds.), *Landscapes and landforms of Italy. World geomorphological landscape* (pp. 203–213). Springer International Publishing AG. https://doi.org/10.1007/978-3-319-26194-2_17.

Pepe, G., Mandarino, A., Raso, E., Scarpellini, P., Brandolini, P., & Cevasco, A. (2019). Investigation on farmland abandonment of terraced slopes using multitemporal data sources comparison and its implication on hydro-geomorphological processes. *Water, 11*, 1552. https://doi.org/10.3390/w11081552

Persichillo, M. G., Bordoni, M., Cavalli, M., Crema, S., & Meisina, C. (2018). The role of human activities on sediment connectivity of shallow landslides. *Catena, 160*, 261–274. https://doi.org/10.1016/j.catena.2017.09.025

Pittau, S., Pizziolo, M., Rossi, M., & Brardinoni, F. (2021). A multi-temporal mapping approach for improving the temporal and spatial characterization of landslide activity in clay-rich terrain. *RENDICONTI ONLINE DELLA SOCIETÀ GEOLOGICA ITALIANA, 54*, 17–31. https://doi.org/10.3301/ROL.2021.06

Podobnikar, T. (2009). Methods for visual quality assessment of a digital terrain model. *Surveys and Perspectives Integrating Environment and Society, 2*(2).

Poeppl, R. E., Polvi, L. E., & Turnbull, L. (2023). (Dis)connectivity in hydro-geomorphic systems – emerging concepts and their applications. *Earth Surface Processes and Landforms, 48*, 1089–1094. https://doi.org/10.1002/esp.5574

Poesen, J., Nachtergaele, J., Verstraeten, G., & Valentin, C. (2003). Gully erosion and environmental change: Importance and research needs. *Catena, 50*(2–4), 91–133. https://doi.org/10.1016/S0341-8162(02)00143-1

Rainato, R., Picco, L., Cavalli, M., Mao, L., Neverman, A. J., & Tarolli, P. (2018). Coupling climate conditions, sediment sources and sediment transport in an Alpine basin. *Land Degradation & Development, 29*, 1154–1166. https://doi.org/10.1002/ldr.2813

Regione Emilia-Romagna. (1994). I suoli dell'Emilia-Romagna. Note Illustrative. *Servizio Cartografico – Ufficio Pedologico*, pp. 383.

Regione Emilia-Romagna. (2019). Modello Digitale del Terreno 5x5, Edizione 2014. *Archivio cartografico*. Geoportale Regione Emilia-Romagna. https://www.geoportale.regione.emilia-romagna.it/catalogo/dati-cartografici/altimetria/layer-2.

Regione Emilia-Romagna. (2020a). *DBTR – Carta Tecnica Regionale 1:5000. Settore innovazione digitale, dati, tecnologia e polo archivistico*. Geoportale Regione Emilia-Romagna. https://www.geoportale.regione.emilia-romagna.it/catalogo/dati-cartografici/cartografia-di-base/cartografia-tecnica/layer-1.

Regione Emilia-Romagna. (2020b). Coperture vettoriali uso del suolo di dettaglio 2017 – Edizione 2020. *Settore innovazione digitale, dati, tecnologia e polo archivistico*. Geoportale Regione Emilia-Romagna. https://geoportale.regione.emilia-romagna.it/catalogo/dati-cartografici/pianificazione-e-catasto/uso-del-suolo/layer-9.

Renard, K. G., Foster, G. R., Weesies, G. A., McCool, D. K., & Yoder, D. C. (1997). Predicting soil erosion by water: A guide to conservation planning with the revised universal soil loss equation (rusle). In *USDA, agriculture handbook* (Vol 703). Washington, DC: US Government Printing Office.

Sartirana, D., Rotiroti, M., Zanotti, C., Bonomi, T., Fumagalli, L., & De Amicis, M. (2020). A 3D geodatabase for urban underground infrastructures: Implementation and application to groundwater management in milan metropolitan area. *ISPRS International Journal of Geo-Information, 9*(10), 609. https://doi.org/10.3390/ijgi9100609

Schmaltz, E. M., Johannesen, L. L., Thorsøe, M. H., Tähtikarhu, M., Räsänen, T. A., Darboux, F., & Strauss, P. (2024). Connectivity elements and mitigation measures in policy-relevant soil erosion models: A survey across europe. *Catena, 234*, Article 107600. https://doi.org/10.1016/j.catena.2023.107600

Schneider, M., Cotton, F., & Johanna-Schweizer, P. (2023). Criteria-based visualization design for hazard maps. *Natural Hazards and Earth System Sciences, 23*, 2505–2521. https://doi.org/10.5194/nhess-23-2505-2023

Servizio Geologico d'Italia. (1999). *Carta Geologica d'Italia alla scala 1:50000, Foglio 198 - Bardi*. Roma: Istituto Poligrafico e Zecca dello Stato.

SGSS - Servizio Geologico, Sismico e dei Suoli. (2005). Banca dati geologica, 1:10000 – Frane, depositi di versante e depositi alluvionali – 10k. *Regione Emilia-Romagna. Geoportale Regione Emilia-Romagna*. https://geoportale.regione.emilia-romagna.it/catalogo/dati-cartografici/informazioni-geoscientifiche/geologia/banca-dati-geologica-1-10.000/layer-4.

Simoni, A., Ponza, A., Picotti, V., Berti, M., & Dinelli, E. (2013). Earthflow sediment production and Holocene sediment record in a large Apennine catchment. *Geomorphology, 188*, 42–53. https://doi.org/10.1016/j.geomorph.2012.12.006

Staffilani, F., Bonaposta, D., & Marucci, F. E. (2019). Carta dell'Erosione idrica attuale della Regione emilia-romagna. *Servizio Geologico, Sismico e Suoli. Regione Emilia-Romagna*.

Steger, S., Scorpio, V., Comiti, F., & Cavalli, M. (2022). Data-driven modelling of joint debris flow release susceptibility and connectivity. Earth Surf. Process. *Landforms, 47*(11), 2740–2764. https://doi.org/10.1002/esp.5421

Strahler, A. N. (1957). Quantitative analysis of watershed geomorphology. *Transactions - American Geophysical Union, 38*(6), 913–920. https://doi.org/10.1029/TR038i006p00913

Tangi, M., Schmitt, R., Bizzi, S., & Castelletti, A. (2019). The CASCADE toolbox for analyzing river sediment connectivity and management. *Environmental Modelling & Software, 119*, 400–406. https://doi.org/10.1016/j.envsoft.2019.07.008

Tarboton, D. G. (1997). A new method for the determination of flow directions and upslope areas in grid digital elevation models. *Water Resources Research, 33*(2), 309–319. https://doi.org/10.1029/96WR03137

Theler, D., Reynard, E., Lambiel, C., & Bardou, E. (2010). The contribution of geomorphological mapping to sediment transfer evaluation in small alpine catchments. *Geomorphology, 124*, 113–123. https://doi.org/10.1016/j.geomorph.2010.03.006

Torresani, L., Piton, G., & D'Agostino, V. (2023). Morphodynamics and sediment connectivity index in an unmanaged, debris-flow prone catchment: A through time perspective. *Journal of Mountain Science, 20*(4), 891–910. https://doi.org/10.1007/s11629-022-7746-2

Trigila, A., Iadanza, C., & Rischia, I. (2007). Metodologia di lavoro e struttura della banca dati. Agenzia per la Protezione dell'Ambiente e per i Servizi Tecnici. In *Rapporto sulle frane in Italia. Il Progetto IFFI – Metodologia, risultati e rapporti regionali* (pp. 3–30). Rapporti APAT 78/2007, Roma.

Trigila, A., Iadanza, C., & Spizzichino, D. (2010). Quality assessment of the Italian Landslide Inventory using GIS processing. *Landslides, 7*, 455–470. https://doi.org/10.1007/s10346-010-0213-0

Turley, M., & Hassan, M. A. (2023). Spatial patterns of disconnectivity explain catchment-scale sediment dynamics and transfer efficiencies. *Journal of Geophysical Research: Earth Surface, 128*, Article e2023JF007111. https://doi.org/10.1029/2023JF007111

Ubaldi, D., Puppi, G., & Zanotti, A. L. (1996). Cartografia fitoclimatica dell'Emilia-Romagna in scala 1:500000. In *Collana Studi e Documentazioni* (Vol 47). Bologna: Regione Emilia-Romagna.

Van Rompaey, A., Bazzoffi, P., Jones, R. J. A., & Montanarella, L. (2005). Modeling sediment yields in Italian catchments. *Geomorphology, 65*, 157–169. https://doi:10.1016/j.geomorph.2004.08.006.

Varnes, D. J. (1978). Slope movements types and processes. In R. L. Schuster, & R. J. Krizek (Eds.), *Landslides: Analysis and control (special report 176)* (pp. 11–33). Washington: Transportation Research Board, National Academy of Science.

Verstraeten, G., Bazzoffi, P., Lajczak, A., Radoane, M., Rey, F., Poesen, J., & de Vente, J. (2006). Reservoir and pond sedimentation in Europe. In J. Boardman, & J. Poesen (Eds.), *Soil erosion in europe* (pp. 759–774). Chichester: Wiley.

Wainwright, J., Turnbull, L., Ibrahim, T. G., Lexartza-Artza, I., Thornton, S. F., & Brazier, R. E. (2011). Linking environmental régimes, space and time: Interpretations of structural and functional connectivity. *Geomorphology, 126*, 387–404. https://doi.org/10.1016/j.geomorph.2010.07.027

Walling, D. E. (1983). The sediment delivery problem. *Journal of Hydrology, 65*(1–3), 209–237. https://doi.org/10.1016/0022-1694(83)90217-2

Wang, L., & Liu, H. (2006). An efficient method for identifying and filling surface depressions in digital elevation models for hydrologic analysis and modelling. *International Journal of Geographical Information Science, 20*(2), 193–213. https://doi.org/10.1080/13658810500433453

Wichmann, V., Heckmann, T., Haas, F., & Becht, M. (2009). A new modelling approach to delineate the spatial extent of alpine sediment cascades.

Geomorphology, 111, 70–78. https://doi.org/10.1016/j.geomorph.2008.04.028

Wischmeier, W. H., & Smith, D. D. (1978). Predicting rainfall erosion losses - a guide to conservation planning. In *Agriculture handbook No.* (Vol 537). Washington DC: US Department of Agriculture.

Wohl, E., Brierley, G., Cadol, D., Coulthard, T. J., Covino, T., Fryirs, K. A., Grant, G., Hilton, R. G., Lane, S. N., Magilligan, F. J., Meitze, K. M., Passalacqua, P., Poeppl, R. E., Rathburn, S. L., & Sklar, L. S. (2019). Connectivity as an emergent property of geomorphic systems. *Earth Surface Processes and Landforms, 44*, 4–26. https://doi.org/10.1002/esp.4434

Woznicki, S. A., Cada, P., Wickham, J., Schmidt, M., Baynes, J., Mehaffey, M., & Neale, A. (2020). Sediment retention by natural landscapes in the conterminous United States. *The Science of the Total Environment, 745*. https://doi.org/10.1016/j.scitotenv.2020.140972

WP/WLI - International Geotechnical Societies UNESCO Working Party on World Landslide Inventory. (1990). A suggested method for reporting a landslide. *Bulletin of the International Association of Engineering Geology, 41*, 5–12.

WP/WLI - International Geotechnical Societies UNESCO Working Party on World Landslide Inventory. (1991). A suggested method for a landslide summary. *Bulletin of the International Association of Engineering Geology, 43*, 101–110.

WP/WLI - International Geotechnical Societies UNESCO Working Party on World Landslide Inventory. (1993a). A suggested method for describing the activity of a landslide. *Bulletin of the International Association of Engineering Geology, 47*, 53–57.

WP/WLI - International Geotechnical Societies UNESCO Working Party on World Landslide Inventory. (1993b). *Multilingual landslide glossary* (p. 59). Richmond, British Columbia, Canada: Bitech Publisher.

WP/WLI - International Geotechnical Societies UNESCO Working Party on World Landslide Inventory. (1994). A suggested method for reporting landslide causes. *Bulletin of the International Association of Engineering Geology, 50*, 71–74.

Yu, Y., Feng, J., Liu, H., Wu, C., Zhang, J., Wang, Z., Liu, C., Zhao, J., & Rodrigo-Comino, J. (2023). Linking hydrological connectivity to sustainable watershed management in the Loess Plateau of China. *Current Opinion in Environmental Science Health, 35*, Article 100493. https://doi.org/10.1016/j.coesh.2023.100493

Zanandrea, F., Michel, G. P., Kobiyama, M., & Cardozo, G. L. (2019). Evaluation of different DTMs in sediment connectivity determination in the Mascarada River Watershed, southern Brazil. *Geomorphology, 332*, 80–87. https://doi.org/10.1016/j.geomorph.2019.02.005

Zevenbergen, L. W., & Thorne, C. R. (1987). Quantitative analysis of land surface topography. *Earth Surface Processes and Landforms, 12*(1), 47–56. https://doi.org/10.1002/esp.3290120107

Zhao, G., Gao, P., Tian, P., Sun, W., Hu, J., & Mu, X. (2020). Assessing sediment connectivity and soil erosion by water in a representative catchment on the Loess Plateau, China. *Catena, 185*, Article 104284. https://doi.org/10.1016/j.catena.2019.104284

Zingaro, M., Refice, A., Giachetta, E., D'Addabbo, A., Lovergine, F., De Pasquale, V., Pepe, G., Brandolini, P., Cevasco, A., & Capolongo, D. (2019). Sediment mobility and connectivity in a catchment: A new mapping approach. *The Science of the Total Environment, 672*, 763–775. https://doi.org/10.1016/j.scitotenv.2019.03.461